J. Fluid Mech. (2004), *vol.* 507, *pp.* 335–366.
DOI: 10.1017/S0022112004008808 Printed in the United Kingdom

On the unsteady motion of a long fluid-loaded elastic plate with mean flow

By N. PEAKE

Department of Applied Mathematics and Theoretical Physics, University of Cambridge, Centre for Mathematical Sciences, Wilberforce Road, Cambridge CB3 0WA, UK

(Received 13 May 2002 and in revised form 24 July 2003)

In this paper we consider the dynamic behaviour of a fluid-loaded elastic plate of dimensionless length $2L$, set in a rigid baffle in the presence of uniform mean flow of dimensionless speed U, and including plate pre-tension (dimensionless tension T) and a spring foundation (dimensionless spring constant λ). Our aim is to extend previous analytical work of Crighton & Oswell (1991), who examined an infinite plate with $T = \lambda = 0$. This is achieved by considering a plate which is long on the scale of typical plate bending waves, and then by expressing the unsteady motion as a superposition of infinite-plate waves which are continuously rescattered in near-field regions at the plate leading and trailing edges. We find that the finite plate possesses resonant solutions which are temporally unstable, both for parameter values for which the infinite plate is convectively unstable (T and/or λ sufficiently small) and parameter values for which it is stable (T and/or λ sufficiently large). It is shown that instability is present in the absence of structural damping on the finite plate, in agreement with numerical results of Lucey & Carpenter (1992). Neutral resonant states are also found, for which we derive a generalization of the Landahl (1962) and Benjamin (1963) concept of wave energy. Finally, we replace the linear pre-tension T by the nonlinear tension induced by bending, and analyse the nonlinear evolution of the states of negative wave energy in the presence of weak structural damping. We show that the system possesses points of minimum action at non-zero frequency, which act as attractors, predicting the existence of nonlinear fluttering motion.

1. Introduction

The stability of a compliant plate immersed in a moving fluid is of fundamental importance to the operation of a range of engineering systems, and has received a very great deal of attention in the literature. Three different theoretical approaches to the problem will be identified here. First, the Galerkin method is used to study walls of finite length, e.g. Ellen (1973, 1977), Kornecki (1974), Dowell (1975), Lucey & Carpenter (1993). The approach here has been to make a truncated (often Fourier) series expansion, and typically then to seek a minimum flow speed for the existence of static divergence (zero-frequency solution) or flutter. Second, in so-called 'travelling-wave' analysis, e.g. Landahl (1962), Carpenter & Garrad (1985, 1986), one considers wave motion on infinitely long plates. The most basic problem in this area, namely uniform mean flow over an elastic plate in two dimensions, has received the most detailed attention, including by Brazier-Smith & Scott (1984), Crighton & Oswell (1991) and Abrahams & Wickham (2001). In a third approach, direct numerical solution of the unsteady plate equation for a finite baffle can be completed, e.g. Lucey &

Carpenter (1992) and Lucey (1998) for linear motion, and Lucey *et al.* (1997) for nonlinear motion. The aim of the current paper is to use elements of the second approach, but to extend it to the case of a finite plate so as to allow more proper comparison with results from the third, numerical approach. This will be achieved by considering the limit in which the plate length is very long, but finite, on the lengthscale of typical plate bending waves.

The resonance of a finite fluid-loaded plate with zero mean flow has been investigated in a number of ways, but we mention especially here the work of Abrahams (1981), who considers a long plate and uses matched asymptotic expansions and Wiener–Hopf analysis to study the local reflection of infinite-plate waves at the two ends separately. This work provides the inspiration for the technique to be applied here. In zero mean flow, Abrahams shows that the resonant frequencies are proportional to the 5/2 power of the inverse plate length. This case is relevant to the high-frequency behaviour of a finite plate with non-zero flow, in which case the effects of the mean flow are not felt to leading order. In contrast, with non-zero mean flow the plate can experience low-frequency divergence instability, and for a given flow speed states of static divergence are possible for a set of discrete values of plate length, as identified by Ellen (1973) using the Galerkin technique and Abrahams (1983) using the same long-plate approximation as mentioned above. One aim of the present work is to map out the behaviour of resonant states with frequencies intermediate between these two limits.

The specific problem we consider is a thin elastic plate of dimensionless length $2L$, with uniform mean flow, dimensionless speed U, on one side and a spring foundation, dimensionless spring constant λ, on the other. In the first instance the plate has linear pre-tension, of dimensionless size T, which is subsequently replaced by the nonlinear tension due to bending. This is therefore a model of the sort of compliant panel famously studied by Kramer (1960). We present the formulation of this problem in § 2. In § 3 we describe for completeness those aspects of the solution of the infinite elastic plate with uniform mean flow which will be required subsequently. In § 4 we present the leading- and trailing-edge scattering problems, which are combined to provide both the forced response of the plate and the conditions for resonance. In § 5 full results for the occurrence of resonance are presented, and we demonstrate the existence of a number of different families of resonant modes. In § 6 we turn our attention to the concept of wave energy – the wave energy of an infinite plate was introduced by Landahl (1962) and Benjamin (1963), but here we extend this concept to the finite plate. All the analysis in §§ 1–6 uses a linear plate equation, but in § 7 we investigate the effects of replacing the linear pre-tension T by the nonlinear tension induced by bending, in an analogous way to Peake (2001) on the infinite plate. Our aim here is to study the nonlinear evolution of negative-energy solutions under the influence of structural damping. In § 8 we discuss further implications of our analysis, and attempt to draw parallels with previous work.

2. Problem formulation

Consider a thin elastic plate, of length $2L_*$ (the star will be used to denote dimensional quantities), which is fixed within an infinitely long rigid baffle – see figure 1. The origin of coordinates is chosen to be at the centre of the undeflected plate, with the x_*-axis aligned along the plate. We suppose that the plate has an infinite span, so that all subsequent motion is two-dimensional and dependence on the spanwise coordinate z_* can be suppressed. Above the plate, in $y_* > 0$, there is

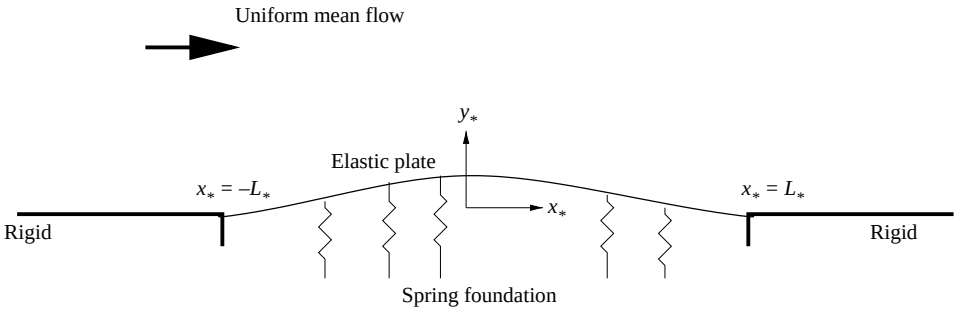

FIGURE 1. The geometry of the finite elastic plate with spring foundation in a rigid baffle.

a fluid which is in uniform motion with steady speed U_* in the x_*-direction, and the plate is supported by a spring foundation in $y_* < 0$. The plate will be forced into motion by the introduction of a line force at the origin, acting in the vertical direction, which is switched on at some initial instant in time $t_* = 0$. The plate deflection in the y_*-direction is denoted by $\eta_*(x_*, t_*)$, and assuming in the first instance that this deflection is small, it is taken to satisfy the linear thin-plate equation (see, for instance, Junger & Feit 1986; Carpenter & Garrad (1985, 1986). Before stating this equation, we will follow Crighton & Oswell (1991) and non-dimensionalize all lengths by m_*/ρ_*^f, where m_* is the plate mass per unit area and ρ_*^f is the fluid density, while time is non-dimensionalized by $m_*^{5/2}/(\rho_*^f)^2 B_*^{1/2}$, where B_* is the plate bending stiffness. The non-dimensional plate equation is then

$$\frac{\partial^4 \eta}{\partial x^4} + \frac{\partial^2 \eta}{\partial t^2} - T\frac{\partial^2 \eta}{\partial x^2} + \lambda \eta = -p(x, 0, t) + F_0(t)\delta(x). \tag{2.1}$$

Here $p(x, y, t)$ is the non-dimensional hydrodynamic pressure (specifically, the dimensional hydrodynamic pressure is $p_* = B_*(\rho_*^f/m_*)^3 p$). We assume that the fluid above the plate is inviscid, incompressible and irrotational, so that the fluid motion is described by the non-dimensional velocity potential $\phi(x, y, t)$ (specifically, the dimensional potential is $\phi_* = (B_*/m_*)^{1/2}\phi$), which satisfies Laplace's equation

$$\nabla^2 \phi = 0. \tag{2.2}$$

The fluid pressure is then given by the linearized Bernoulli relation

$$p = -\left(\frac{\partial \phi}{\partial t} + U\frac{\partial \phi}{\partial x}\right), \tag{2.3}$$

where U is now the non-dimensional mean-flow velocity $U = U_* m_*^{3/2}/\rho_*^f B_*^{1/2}$. In (2.1) the third term on the left-hand side represents the effects of the elastic plate being pre-tensioned before the motion is initiated, with T the non-dimensional pre-tension. We will consider later the effects of the tension induced by nonlinear bending of the plate, but within the purely linear context of this section a tension term can only be included as a result of external pre-tensioning. In (2.1) the fourth term on the left represents the effects of the spring foundation, with dimensionless spring constant $\lambda = K_*^E m_*^4/(\rho_f^4 B_*)$. Here, K_*^E is the effective dimensional spring constant, which incorporates the effects of both the spring foundation and the hydrostatic pressure variations as the plate moves (see Carpenter & Garrad 1986, p. 202, for details). The boundary conditions are that the normal component of the fluid velocity

must vanish on the rigid baffle, i.e.

$$\frac{\partial \phi}{\partial y} = 0 \quad \text{on} \quad y = 0 \quad \text{when} \quad |x| > L, \tag{2.4}$$

and that the elastic plate moves with the local fluid velocity in the y-direction, so that

$$\frac{\partial \phi}{\partial y} = \frac{\partial \eta}{\partial t} + U\frac{\partial \eta}{\partial x} \quad \text{on} \quad y = 0 \quad \text{when} \quad |x| < L. \tag{2.5}$$

Finally, we specify clamped conditions at the two ends of the elastic plate, so that

$$\eta = \frac{\partial \eta}{\partial x} = 0 \quad \text{when} \quad x = \pm L. \tag{2.6}$$

Equations (2.1)–(2.6) specify the problem to be studied in this paper. It turns out that they can be condensed into a single equation for the plate deflection, by using Green's theorem to write the solution of Laplace's equation with boundary data (2.4) and (2.5) in the form of an integral over the plate. Specifically, we find that

$$p(x, 0, t) = -\frac{1}{\pi}\int_{-L}^{L} \ln|x - \xi| \left(\frac{\partial}{\partial t} + U\frac{\partial}{\partial \xi}\right)^2 \eta(\xi, t)\, \mathrm{d}\xi, \tag{2.7}$$

and substituting this into (2.1) yields

$$\mathscr{L}\eta \equiv -\frac{\partial^2 \eta}{\partial t^2} - \frac{\partial^4 \eta}{\partial x^4} + T\frac{\partial^2 \eta}{\partial x^2} - \lambda\eta + \frac{1}{\pi}\int_{-L}^{L} \ln|x-\xi| \left(\frac{\partial}{\partial t} + U\frac{\partial}{\partial \xi}\right)^2 \eta(\xi, t)\, \mathrm{d}\xi = -F_0(t)\delta(x). \tag{2.8}$$

In our subsequent analysis we will make use of both this latter result and the primitive equations (2.1)–(2.6).

3. Solution for an infinitely long plate

Since our solution for a long, but finite elastic plate will be built up in part from the motions allowed on an infinite plate, we will first review the wave properties of our system when $L \to \infty$.

3.1. *Dispersion relation*

By considering solutions proportional to $\exp(-\mathrm{i}\omega t + \mathrm{i}kx)$, it is straightforward to show from (2.1)–(2.3), and (2.5) applied for all x, that the waves on an infinite elastic plate satisfy the dispersion relation

$$\mathscr{D}(k, \omega) \equiv \omega^2 + \frac{(\omega - kU)^2}{\gamma(k)} - k^4 - Tk^2 - \lambda = 0, \tag{3.1}$$

where $\gamma(k) \equiv \sqrt{k^2}$ (denoted $|k|$ by Crighton & Oswell) is defined by introducing branch cuts joining $0 \pm 0\mathrm{i}$ to infinity along the positive and negative imaginary axes, with $\gamma(k)$ positive on the real-k-axis. The case $T = \lambda = 0$ is considered by Brazier-Smith & Scott (1984), and in great detail by Crighton & Oswell (1991), while more recently de Langre (2002) has considered $T \neq 0$.

The long-time causal behaviour of an infinite plate with a line driver can be determined using the Briggs–Bers technique (Briggs 1964; Bers 1983). Full details of this method applied in the present context have been given a number of times previously (see Crighton & Oswell 1991 for example), and only the briefest outline is necessary here. Starting with $\mathrm{Im}(\omega)$ large and positive, the motion of the spatial

roots of (3.1) is tracked as $\mathrm{Im}(\omega)$ is reduced to zero. Absolute instability occurs if two spatial roots originating from different halves of the k-plane collide for $\mathrm{Im}(\omega) > 0$. If $\mathrm{Im}(\omega)$ can be reduced to zero without such a collision, the system is at worst convectively unstable; a convectively unstable mode is one which crosses the real-k-axis from above, and comes to rest with $\mathrm{Im}(k) < 0$ when ω is real. Neutral modes come to rest on the real-k-axis when ω is real, and the half-plane from which they originate determines their spatial location; neutral modes originating from the upper half of the k-plane are located downstream of the driver (i.e. $x > 0$), while neutral modes originating from the lower half of the k-plane are located upstream of the driver (i.e. $x < 0$). Finally, we note that modes which do not reach the real-k-axis once ω becomes real are evanescent – if $\mathrm{Im}(k) > 0$ evanescent downstream of the driver, and if $\mathrm{Im}(k) < 0$ evanescent upstream of the driver.

Crighton & Oswell (1991) show that when $T = \lambda = 0$ the infinite plate is absolutely unstable if $U > 0.0742\ldots$, while de Langre (2002) demonstrates that this boundary rises rapidly to higher U as the pre-tension is increased, approaching the corresponding value for a membrane as $T \to \infty$ (see Kelbert & Sazanov 1996). Throughout this paper we will assume that we are below the absolute instability threshold, which then allows us to plot spatial dispersion diagrams, of $k(\omega)$ against real ω, and two examples are shown in figure 2.

It turns out that for real ω there are typically four valid k-roots of (3.1). Two types of behaviour are possible:

(*a*) When both T and λ are sufficiently small, the behaviour shown in figure 2(*a*) applies, in which there are two quite distinct looping branches of neutral waves. When $0 < \omega < \omega_a(U, T, \lambda)$ there are four neutral modes, two located upstream and two located downstream according to the Briggs–Bers analysis. When $\omega_a(U, T, \lambda) < \omega < \omega_s(U, T, \lambda)$ there are two neutral modes, both located downstream, and a pair of complex-conjugate modes, both located upstream of the driver, the one with $\mathrm{Im}(k) < 0$ corresponding to a convective instability and the one with $\mathrm{Im}(k) > 0$ being evanescent. There are four neutral modes in the frequency range $\omega_s(U, T, \lambda) < \omega < \omega_p(U, T, \lambda)$, two located downstream of the driver and two located upstream. Briggs–Bers analysis shows that the spatial location of these neutral modes is given by their local group velocity (i.e. by the gradient of the curve in figure 2*a*), except for the mode with $k_b(U, T, \lambda) < k < k_s(U, T, \lambda)$ when $\omega < \omega_b(U, T, \lambda)$. This latter mode is described by Crighton & Oswell (1991) as being 'anomalous', in that it is located downstream of the driver, even though its group velocity points upstream. For $\omega > \omega_p(U, T, \lambda)$ there are two neutral modes, one downstream and one upstream, and again a pair of complex-conjugate modes, but this time both evanescent (one upstream and one downstream).

(*b*) As either T or λ is increased from the values shown in figure 2(*a*), the points $(k_{a,s}, \omega_{a,s})$ move towards each other, reducing the frequency range over which the plate is convectively unstable, until the two looping branches merge and the convectively unstable region vanishes completely – see figure 2(*b*). For $0 < \omega < \omega_p(U, T, \lambda)$ there are then four neutral modes, two upstream and two downstream; the anomalous mode has now disappeared, so that all four modes have group velocity pointing away from the driver. For $\omega > \omega_p(U, T, \lambda)$ the situation is exactly as in figure 2(*a*), with two neutral modes and two evanescent modes. Different behaviour is possible when λ is increased significantly higher than the case shown in figure 2(*b*), but we will not concern ourselves with such a situation here.

The range of U–T–λ parameter space over which the plate is convectively unstable cannot be determined in closed form in general, although we note that in the special

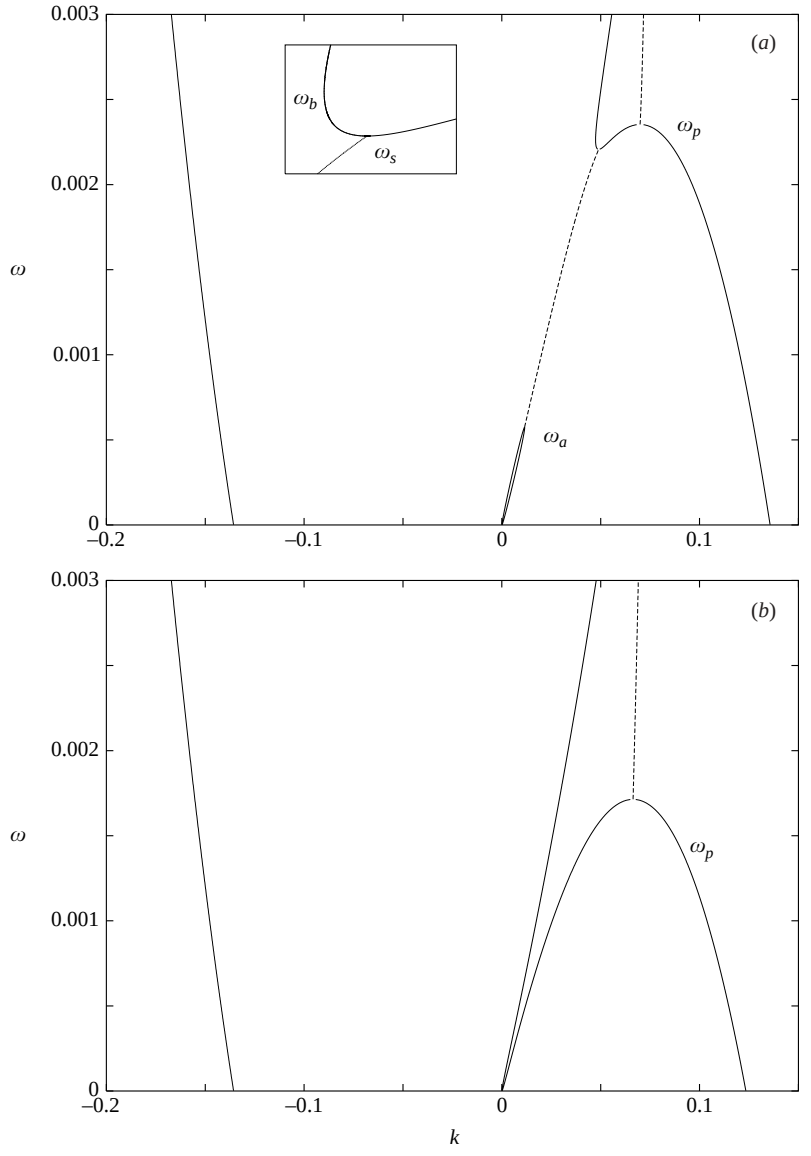

FIGURE 2. The dispersion diagram for the infinite plate. Plotted are solutions $k(\omega)$ of $\mathscr{D}(k, \omega) = 0$ for real positive ω; note that roots for negative ω can be determined from $\mathscr{D}(k, \omega) = \mathscr{D}(-k, -\omega)$. Here the flow speed is $U = 0.05$, the spring constant is $\lambda = U^5$ and (*a*) $T = 0$, (*b*) $T = 2U^2$. The solid lines denote neutral modes, and the dashed lines denote Re(k) for complex modes. The inset in (*a*) shows a magnified view of the region around $\omega_{s,b}$.

case $\lambda = 0$ the frequency $\omega_a \to 0$ and the convective instability boundary is $T = U^2$. In summary, in the cases shown in figure 2 there are four modes allowed on the infinite plate, two of them located downstream of the driver and two upstream. We shall refer to the two downstream waves as $k^+_{1,2}$ and to the two upstream waves as $k^-_{1,2}$.

3.2. *Limit of small U*

Crighton & Oswell (1991) showed that considerable simplification of the infinite-plate problem is possible in the limit of small non-dimensional flow speed, $U \ll 1$ (this is a

reasonable limit which covers many cases of practical interest, not least because the boundary for absolute instability is at $U = 0.0742\ldots$). This limit will be helpful in what follows, and we therefore summarize here the scalings which apply to the roots of (3.1) in this limit. When the plate is convectively unstable (figure 2*a*), the convectively unstable region $\omega_a(U, T, \lambda) < \omega < \omega_s(U, T, \lambda)$ is described by the scaling $\omega = O(U^2)$. Consequently, the convectively unstable modes have wavenumber $k = O(U)$, with $k \sim \omega/U$, while the neutral modes have $k = O(U^{2/3})$. The neutral region around $\omega_s(U, T, \lambda)$ and $\omega_b(U, T, \lambda)$ is also described by $\omega = O(U^2)$, with the same scalings of the corresponding wavenumbers. The frequency range around the higher turning point $\omega_p(U, T, \lambda)$ has $\omega = O(U^{5/3})$, and all the neutral waves here have $k = O(U^{2/3})$.

We can derive a small-U expression for the boundary in T–λ space of the convectively unstable region. We start by writing $k = UK$, $\omega - Uk = \Omega U^{5/4}$, $T = U^2\tau$, $\lambda = \Lambda U^4$, with $K, \Omega, \tau, \Lambda = O(1)$, and substituting into the dispersion relation (3.1) shows that $\Omega = \sqrt{K}\sqrt{K^4 + (\tau - 1)K^2 + \Lambda}$. Hence, the condition for convective instability is that Ω is complex for some K, i.e.

$$T < U^2 - 2\sqrt{\lambda}. \tag{3.2}$$

When there is no convective instability (figure 2*b*) then in the range $\omega = O(U^2)$ two neutral modes have $k \sim \omega/U$ and two have $k = O(U^{2/3})$, while the remaining turning point $\omega_p(T, U, \lambda)$ is described by the same scaling as for the convectively unstable case.

In order to be able to consider the leading- and trailing-edge regions separately, we need the plate to be long on the scale of the wavelengths of the allowed infinite-plate waves. This condition can be quantified using the orders of magnitude stated in the previous paragraph. For instance, for $\omega = O(U^2)$ we have two waves with a wavenumber (with real part) $O(\omega/U)$ and two waves of wavenumber $O(U^{2/3})$. In this range we therefore require $LU^{2/3} \gg 1$ and $\omega L/U \gg 1$. Alternatively, for $\omega = O(U^{5/3})$, all four modes have $k = O(U^{2/3})$ so that we just require the single condition $LU^{2/3} \gg 1$.

We have now completed our description of the wave-bearing properties of an infinite elastic plate, and in the next section we use this information to construct solutions for our finite-plate problem.

4. Unsteady solution

In this section we present the unsteady solution. We consider first the reflection properties of the two edges, before adding in the line driver in § 4.3. We will be looking for solutions with a single frequency, ω, not necessarily real (either a resonant frequency or the frequency imposed by the line driver), and in what follows we therefore suppose that all unsteady quantities are proportional to the factor $\exp(-\mathrm{i}\omega t)$, which will be suppressed.

Because the elastic plate is long, the unsteady plate deflection over most of the plate will be given in terms of the allowed wave motions on an infinitely long plate, as described in the previous section. Of course, this approximation will not hold within inner, or near-field, regions around each edge, whose size scales on the typical wavelengths present on the plate. The wave approximation will also fail in an inner region around the line drive, which also possesses a near field. We can therefore think of an outer region along most of the plate in which the plate deflection, and the velocity potential associated with that deflection, can be written as sums of infinite-plate waves. At each point in the outer region there will be two upstream and two downstream waves. The amplitudes of these waves are at this stage unknown, and

will take different values upstream and downstream of $x = 0$, thanks to the presence of the line driver.

The idea of splitting the plate into inner regions around each edge and an outer region comprising the rest of the plate has been exploited by Abrahams, who considered an elastic plate in a rigid baffle with zero mean flow (Abrahams 1981), and non-zero mean flow (Abrahams 1983). In these papers, the method of matched asymptotic expansions was performed in the limit of heavy fluid loading. Abrahams considers compressible flow, and uses an asymptotic parameter based on the fluid sound speed, which is different from the incompressible problem studied here. However, it is clear from Abrahams' detailed analysis that for a long plate one considers the reflection problems at the leading and trailing edges separately. At the leading edge upstream modes are reflected into downstream modes, and vice versa at the trailing edge, and the consistency of these two scattering problems then leads to a condition for plate resonance.

4.1. *Leading-edge problem*

We first consider scattering of the upstream waves by the leading edge, with the trailing edge ignored and the elastic plate extending to infinity in the downstream direction. We start by introducing the shifted coordinate $x' = x + L$, and the total plate deflection and associated fluid potential are then written in the form

$$\left.\begin{aligned} &\eta_s(x) + \sum_{j=1}^{2} B_j^- \exp(\mathrm{i}k_j^- x'), \\ &\phi_s(x, y) + \sum_{j=1}^{2} \mathrm{i}\frac{(\omega - Uk_j^-)}{\gamma(k_j^-)} B_j^- \exp(\mathrm{i}k_j^- x' - \gamma(k_j^-)y), \end{aligned}\right\} \tag{4.1}$$

respectively. The terms B_j^- represent the amplitudes of the two upstream waves which are incident on the leading edge. The scattered plate deflection $\eta_s(x')$ and potential $\phi_s(x', y)$ must now be chosen to satisfy the boundary condition of zero total normal velocity on $y = 0, x' < 0$, and the elastic plate boundary condition (2.5) on $y = 0, x' > 0$, together with the edge conditions (2.6) at $x' = 0$. The solution of this problem is completed using the Wiener–Hopf technique, and proceeds in much the same way as described by Abrahams (1981), and indeed as described by a number of other authors (e.g. Cannell 1976 and Crighton & Innes 1984), and only brief details need to be given here.

We define the half-range Fourier transforms of the scattered plate deflection and the scattered potential on the rigid baffle as

$$\left.\begin{aligned} \tilde{\eta}_s^-(k) &\equiv \int_0^\infty \eta_t(x') \exp(-\mathrm{i}kx')\mathrm{d}x', \\ \tilde{\phi}_s^+(k, 0) &\equiv \int_{-\infty}^0 \phi_t(x', 0) \exp(-\mathrm{i}kx')\mathrm{d}x', \end{aligned}\right\} \tag{4.2}$$

respectively. The plus and minus superfixes in (4.2) indicate that the expressions are analytic in the upper and lower halves, $R^\pm$, of the complex-k-plane respectively. The precise definition of what constitutes $R^\pm$ depends on the frequency under consideration, and follows from the Briggs–Bers technique. The idea is that when $\mathrm{Im}(\omega)$ is sufficiently large and positive, $R^\pm$ correspond to $\mathrm{Im}(k)$ positive and negative respectively, but that as $\mathrm{Im}(\omega)$ is reduced towards zero the boundary between $R^\pm$ must be deformed to avoid any spatial modes crossing it. For instance, when ω is

real and lies in the range $0 < \omega < \omega_s(U, T, \lambda)$, as in figure 2(*a*), then a convectively unstable mode has crossed over the real-k-axis to lie in $\mathrm{Im}(k) < 0$, so that in this case the boundary between $R^{\pm}$ is deformed off the real axis to lie below this mode, and the convectively unstable mode lies in R^{+}.

After some algebra, and application of the boundary conditions described at the beginning of this subsection, the quantities in (4.2) can be related to each other in the form of the Wiener–Hopf equation

$$\tilde{\eta}_s^-(k)\mathscr{D}^-(k,\omega) - \sum_{j=1}^{2} \mathrm{i}B_j^- \left\{ \frac{\mathscr{D}^-(k,\omega) - \mathscr{D}^-(k_j^-,\omega)}{k - k_j^-} \right\}$$
$$= -\frac{\mathrm{i}(\omega - Uk)}{\mathscr{D}^+(k,\omega)}\tilde{\phi}_s^+(k,0) - \frac{h(k)}{\mathscr{K}^+(k)} + \sum_{j=1}^{2} \frac{\mathrm{i}B_j^-\mathscr{D}^-(k_j^-,\omega)}{(k - k_j^-)} + \frac{(k^4 - \omega^2)}{\mathscr{D}^+(k,\omega)} \sum_{j=1}^{2} \frac{\mathrm{i}B_j^-}{(k - k_j^-)}. \tag{4.3}$$

Here

$$h(k) \equiv \frac{\partial^3 \eta_s}{\partial x^3} + \mathrm{i}k\frac{\partial^2 \eta_s}{\partial x^2} - k^2\frac{\partial \eta_s}{\partial x} - \mathrm{i}k^3\eta_s - U\phi_s \quad \text{on} \quad x' = 0, \tag{4.4}$$

and we use the edge conditions at $x' = 0$ to evaluate two of the unknown quantities in (4.4). The Wiener–Hopf kernel, $\mathscr{D}(k,\omega)$, in (4.3) is precisely the dispersion function given in (3.1). The key step in the Wiener–Hopf technique is the (multiplicative) factorization of this kernel in the form $\mathscr{D}(k,\omega) = \mathscr{D}^+(k,\omega)\mathscr{D}^-(k,\omega)$, where the factors $\mathscr{D}^{\pm}(k,\omega)$ are analytic and non-zero in $R^{\pm}$ respectively. For general values of the frequency the calculation of these factors cannot be completed in closed form, but numerical evaluation is straightforward and details are given in Appendix A. Analytic expressions for $\mathscr{D}^{\pm}(k,\omega)$ can be found for ω small and large, however; the factorization for small ω is described in Appendix A, while the case of larger ω, for which the effects of the mean flow are less important, has been completed by Abrahams (1981).

We now proceed by noting that the left- and right-hand sides of (4.3) are analytic in $R^{\mp}$ respectively, therefore defining by analytical continuation a function, $F(k)$ say, which is analytic throughout the k-plane. By considering the behaviour of (4.3) as $k \to \infty$, noting that $\mathscr{D}^{\pm} \propto k^2$ as $k \to \infty$, and by again using the clamped edge conditions at $x' = 0$, it follows that $F(k) \to 0$ as $k \to \infty$, and so by Liouville's Theorem $F(k) \equiv 0$. An expression for the previously unknown Fourier transform of the scattered plate deflection, $\tilde{\eta}(k)$, can then be found from (4.3) as

$$\tilde{\eta}(k) = -\sum_{j=1}^{2} \frac{\mathrm{i}B_j^-\mathscr{D}^-(k_j^-)}{(k - k_j^-)\mathscr{D}^-(k)}. \tag{4.5}$$

The plate deflection resulting from the scattering of the two upstream waves by the leading edge can now be determined by inverting the Fourier transform (4.5); for $x' > 0$ this is done by closing the inversion contour in the upper half-plane, picking up a branch-line contribution associated with the upper branch cut in $\gamma(k)$, as well as pole contributions from the poles $k = k_{1,2}^+$. The branch-line contribution is associated with the near field around the edge, behaving like $1/x'^{3/2}$ for large $|x'|$, and since we are considering a very long plate the interaction of this near field with the trailing edge will be disregarded. On the other hand, the two pole contributions correspond to

the downstream waves, so that the far-field scattered plate deflection takes the form

$$\sum_{i=1}^{2} B_i^+ \exp(\mathrm{i}k_i^+ x'), \tag{4.6}$$

with a corresponding expression for the associated unsteady potential. The reflected amplitudes of the downstream waves, B_i^+, are related to the incident amplitudes of the upstream waves by

$$B_i^+ = \sum_{j=1}^{2} \mathscr{R}_{ij}^L B_j^-, \tag{4.7}$$

and after a little algebra we find that the leading-edge reflection matrix $\mathscr{R}^L$ has coefficients

$$\mathscr{R}_{ij}^L = \frac{\mathscr{D}^+(k_i^+, \omega)\mathscr{D}^-(k_j^-, \omega)}{\mathscr{D}_k(k_i^+, \omega)(k_i^+ - k_j^-)}, \tag{4.8}$$

where the suffix k denotes differentiation with respect to k. This represents our solution to the leading-edge problem.

4.2. *Trailing-edge problem*

We now consider the scattering of downstream waves at $x = +L$. This is achieved by introducing $x'' = x - L$, and writing the total plate deflection and associated fluid potential in the alternative form (cf. equation (4.1) at the leading edge)

$$\eta_s(x'') + \sum_{j=1}^{2} \bar{B}_j^+ \exp(\mathrm{i}k_j^+ x''), \tag{4.9}$$

$$\phi_s(x'', y) + \sum_{j=1}^{2} \mathrm{i}\frac{(\omega - Uk_j^+)}{\gamma(k_j^+)} \bar{B}_j^+ \exp(\mathrm{i}k_j^+ x'' - \gamma(k_j^+)y), \tag{4.10}$$

where now the $\bar{B}_j^+$ terms represent the incident downstream waves. Exactly the same method is employed here as was employed at the leading edge, and after some algebra we find the final result for the Fourier transform of the scattered plate deflection as

$$\tilde{\eta}(k) = \sum_{j=1}^{2} \frac{\mathrm{i}B_j^+ \mathscr{D}^+(k_j^+)}{(k - k_j^+)\mathscr{D}^+(k)}. \tag{4.11}$$

The amplitudes of the scattered upstream waves are then given by

$$\bar{B}_i^- = \sum_{j=1}^{2} \mathscr{R}_{ij}^T \bar{B}_j^+, \tag{4.12}$$

where the trailing-edge reflection matrix $\mathscr{R}^T$ has coefficients

$$\mathscr{R}_{ij}^T = \frac{\mathscr{D}^+(k_j^+, \omega)\mathscr{D}^-(k_i^-, \omega)}{\mathscr{D}_k(k_i^-, \omega)(k_i^- - k_j^+)}. \tag{4.13}$$

This represents our solution for the trailing-edge problem.

4.3. *Solution and condition for resonance*

We have now derived two results – equations (4.8) and (4.13) – relating amplitudes of the downstream and upstream modes. The condition for resonance will appear explicitly in the solution for the forced problem, which can now be derived in a straightforward manner as follows.

The plate deflection for a line force on an infinite plate is given by Crighton & Oswell (1991). In the far field of the line force the plate deflection is a sum of contributions from infinite-plate waves, and takes the form

$$\left.\begin{aligned} &\sum_{j=1}^{2} h_j^+ \exp(\mathrm{i}k_j^+ x) \quad \text{when} \quad |x| > 0, \\ &\sum_{j=1}^{2} h_j^- \exp(\mathrm{i}k_j^- x) \quad \text{when} \quad |x| < 0, \end{aligned}\right\} \tag{4.14}$$

where

$$h_j^{\pm} = \mp \frac{\mathrm{i}F_0}{\mathscr{D}_k(k_j^{\pm}, \omega)}. \tag{4.15}$$

Here we are considering harmonic forcing, so that F_0 is the strength of the line force. In the presence of this line force, and in the outer region, the deflection of the *finite* plate must take the form

$$\sum_{j=1}^{2}(h_j^+ \mathrm{H}(x) + \alpha_j^+)\exp(\mathrm{i}k_j^+ x) + \sum_{j=1}^{2}(h_j^- \mathrm{H}(-x) + \alpha_j^-)\exp(\mathrm{i}k_j^- x), \tag{4.16}$$

where the unknowns $\alpha_j^{\pm}$ represent corrections to the infinite-plate solution, and the Heaviside functions $\mathrm{H}(\pm x)$ have been introduced to account for the different wave fields upstream and downstream of the line driver. Considering first the leading edge, the incident-wave deflection is $\sum(h_j^- + \alpha_j^-)\exp(\mathrm{i}k_j^- x)$, while the reflected-wave deflection is $\sum \alpha_j^+ \exp(\mathrm{i}k_j^+ x)$, and these can be related using the reflection matrix (4.8). Accounting for the phase factors which relate to the origin shift in § 4.1, we find that, in matrix notation,

$$\underline{\alpha}^+ = \mathscr{S}^L(\underline{h}^- + \underline{\alpha}^-), \tag{4.17}$$

where the matrix $\mathscr{S}^L$ has components

$$\mathscr{S}_{ij}^L = \mathscr{R}_{ij}^L \exp(\mathrm{i}k_i^+ L - \mathrm{i}k_j^- L). \tag{4.18}$$

A similar calculation at the trailing edge yields that

$$\underline{\alpha}^- = \mathscr{S}^T(\underline{h}^+ + \underline{\alpha}^+), \tag{4.19}$$

where the matrix $\mathscr{S}^T$ has components

$$\mathscr{S}_{ij}^T = \mathscr{R}_{ij}^T \exp(-\mathrm{i}k_i^- L + \mathrm{i}k_j^+ L). \tag{4.20}$$

Putting these two results together yields the solution for the unknown quantities $\underline{\alpha}^{\pm}$; for instance

$$\underline{\alpha}^+ = \mathscr{M}^{-1}[\mathscr{S}^L \underline{h}^- + \mathscr{S}^L \mathscr{S}^T \underline{h}^+], \tag{4.21}$$

where

$$\mathscr{M} = \mathscr{I} - \mathscr{S}^L \mathscr{S}^T \tag{4.22}$$

and $\mathscr{I}$ is the 2×2 identity matrix. The condition for plate resonance now follows as

$$\det(\mathscr{M}) = 0. \tag{4.23}$$

Essentially the idea will be that for fixed values of the parameters L, U, T, λ, resonance will occur for an infinite set of discrete, possibly complex, values of ω, and this will be investigated numerically in the next section.

Finally in this section, we note that there are certain real frequencies at which our reflection coefficients appear to be singular, $\omega = \omega_{a,s,p}$, where there are double spatial roots of the dispersion relation $k = k_{a,s,p}$ respectively. This requires further investigation. First, consider $\omega = \omega_p$, which corresponds to a coalescence of a downstream mode (without loss of generality $k = k_1^+$) and an upstream mode (without loss of generality $k = k_1^-$) into the double root $k = k_p$. This point occurs for any pre-tension, see figure 2(a, b). In this case two of the four reflection coefficients at both the leading edge, equation (4.8), and the trailing edge, equation (4.13), appear to be undefined; $R_{12}^{L,T}$ due to $\mathscr{D}_k$ vanishing, and $R_{11}^{L,T}$ due to both $\mathscr{D}_k$ and the second factor in the denominators vanishing. These zeros in the denominator are in fact cancelled by zeros in the numerator from the Wiener–Hopf factors $\mathscr{D}^{\pm}$. It should be noted that in general the Wiener–Hopf factors have been defined to be non-zero. However, we note from equation (A 3) that, for instance, $\mathscr{D}^{\pm}(k_1^{\pm})$ contain factors $(k_1^{\pm} - k_1^{\mp})$ respectively. For general ω these factors are non-zero, but approach zero as $\omega \to \omega_p$, thereby cancelling out the zeros in the denominator of the reflection matrices, and yielding finite leading- and trailing-edge reflection coefficients as $\omega \to \omega_p$. Of course, at exactly $\omega = \omega_p$ coalescence of an upstream and a downstream mode means that our splitting of the plate deflection into upstream and downstream waves is no longer meaningful. But, the crucial result is that our solution to condition (4.23) will vary continuously through $\omega = \omega_p$. Exactly the same sort of behaviour occurs at $\omega = \omega_a$, since the double root $k = k_a$ is also formed by pinching spatial branches.

In contrast, consider the turning point at $\omega = \omega_s$, which corresponds to the coalescence of the two downstream modes ($k = k_{1,2}^+$) (recall that this point only exists for sufficiently low pre-tension, see figure 2a). In this case the apparent singularity arises in the leading-edge coefficients (4.8) only, due to the factor $\mathscr{D}_k(k_i^+, \omega_s)$ becoming zero. This is not cancelled out by zeros in the numerator of (4.8), since this time the double root $k = k_s$ is formed by coalescing roots from the same half-plane, so that the Wiener–Hopf factors remain non-zero as $\omega \to \omega_s$. In fact, in the limit $\omega \to \omega_s$ the individual leading-edge reflection coefficients do indeed approach infinity. However, we can still determine the behaviour of the resonance condition as $\omega \to \omega_s$, by multiplying equation (4.23) by $\mathscr{D}_k(k_1^+, \omega)\mathscr{D}_k(k_2^+, \omega)$ for $\omega \neq \omega_s$ and then taking the limit $\omega \to \omega_s$. Of course, to determine the forced solution at $\omega = \omega_s$ one would need to include secular terms of the form $x \exp(-\mathrm{i}k_s x)$, but we will restrict attention here to the condition for resonance, which (as will be seen in the next subsection) again moves continuously through $\omega = \omega_s$ once the above adjustment has been made.

5. Results for resonance

In this section we will use the result derived in the previous section to describe the possible resonant frequencies of our finite plate. Before considering general values of the frequency, for which the numerical evaluation of the Wiener–Hopf kernel is required, we first mention two special cases of ω very small and ω relatively large, for which considerable simplification is possible.

5.1. *Low-frequency results*

In the case $T=\lambda=0$, Abrahams (1983, equation 4.31) has shown that the low-frequency plate resonances occur at the static divergence conditions

$$k_0 L = \frac{(4n+3)\pi}{8} \tag{5.1}$$

for n any positive integer, where $k_0 = U^{2/3}$. A low-frequency analysis of the result in § 4.3 also yields exactly this result, but details need not be given here. The significance of k_0 is that it is the single positive non-zero wavenumber for $\omega=0$. When $T\neq 0$, $\lambda\neq 0$, such a static divergence wavenumber satisfies the quartic equation

$$k^4 + Tk^2 - U^2 k + \lambda = 0, \tag{5.2}$$

and depending on the values of T, U, λ this equation can have either two or no non-negative real roots. Consider first the limit $\lambda = O(U^4)$, which from (3.2) describes the transition from convective instability to stability on the infinite plate. It follows that to leading order the roots of (5.2) are zero and k_0, where now k_0 is the single real positive root of the cubic equation

$$k^3 + Tk - U^2 = 0. \tag{5.3}$$

It then follows that the value of the pre-tension T will affect the static divergence point k_0 only if $T \geqslant O(U^{4/3})$. When λ increases beyond $O(U^4)$ more complicated behaviour can occur, and indeed for $\lambda \geqslant O(U^{8/3})$ (5.2) may have no positive roots, and static divergence does not occur at all. We will not explore this possibility further here, however, since in this paper we are concerned with the sort of regimes shown in figure 2, in which there is a transition of the infinite plate from convective instability to stability. Putting this information together with Abrahams' result therefore implies that, for the parameter values we consider, the plate resonance lengths at very low frequency will approach the static divergence result (5.1), with k_0 given as the single positive root of (5.3).

5.2. *Higher-frequency results*

When ω is real and significantly larger than ω_p we have just two neutral modes and the evanescent modes can be neglected. Moreover, these neutral modes approximate the bending waves found on a plate in zero flow. To see this we choose the preferred scaling $\omega = O(U)$, $k = O(U^{2/5})$, still with $T = O(U^2)$, $\lambda = O(U^4)$, in which case (3.1) reduces to leading order to

$$\omega^2 - k^4|k| = 0. \tag{5.4}$$

This is the dispersion relation for a plate in zero mean flow, in the low-frequency case in which the plate inertia is negligible compared to fluid loading and bending stiffness. Abrahams considered the reflection of bending waves in zero mean flow, and showed that they are reflected from both the leading and the trailing edges with a reflection coefficient $\exp(3\pi\mathrm{i}/4)$. Since this result is independent of frequency, we can use it in our present limit. For an unforced solution to exist we require that the two bending waves match with each other after one complete passage up and down the plate, and it is easy to show that this corresponds to $-4kL = (3\pi/2) - 2m\pi$ for integer m, or equivalently

$$L = \frac{\left(\frac{1}{2}m\pi - \frac{3}{8}\pi\right)}{\omega^{2/5}}. \tag{5.5}$$

Note that this result is independent of U, T and λ, whose effects would occur at higher order. Also note that (5.5) is valid up to and including $\omega = O(1)$, since the reflection coefficient we used here is frequency-independent. Equation (5.5) is exactly the condition given for standing waves at the end of section 1(e) of Abrahams (1981).

5.3. *Arbitrary frequency results*

In ω–L parameter space we have already seen that resonance exists at very low frequency for values of L approximately independent of ω, equation (5.1), and for larger ω along discrete curves $L \propto \omega^{-2/5}$. The way that these limits join together at intermediate frequencies is the subject of this subsection.

We present specimen plots for the occurrence of resonance in the ω–L plane. Resonance is detected numerically by seeking to maximize the size of the condition number (and minimize the determinant) of the matrix $\mathscr{M}$. The search is conducted through the complex-ω-plane. The lines plotted in figures 3–6 are loci along which $\det\mathscr{M}$ is minimized; the size of these minimum values is typically $O(10^{-10})$ or less, with the corresponding condition number typically at least $O(10^8)$. Exact singularity of $\mathscr{M}$ cannot be achieved, since calculation of the Wiener–Hopf factors requires numerical evaluation of an integral, but we can infer that $\mathscr{M}$ is singular to numerical precision.

In figure 3 we take $T = 0$, $\lambda = U^5$ for which the infinite plate exhibits convective instability when $\omega_a < \mathrm{Re}(\omega) < \omega_s$ (see figure 2*a*). As can be seen, there are two quite distinct families of complex modes, denoted by A (solid lines) and B (dashed lines). Family-A resonances have complex ω for $\omega_a < \mathrm{Re}(\omega) < \omega_s$, but otherwise have ω strictly real, while family B have complex ω all along the dashed curves. Family-B curves merge with the family-A curves at a frequency slightly larger than ω_s, as can be seen clearly in figure 3(*b*). The resonance curves are repeated indefinitely for increasing L, and only a representative sample have been included to demonstrate the behaviour. In figure 4 we plot $\mathrm{Im}(\omega)$ against $\mathrm{Re}(\omega)$ for a typical family-A complex resonance, which is seen to be temporally unstable only for certain ranges of $\mathrm{Re}(\omega)$, or equivalently only for certain values of baffle length, and is damped over the rest of $\omega_a < \mathrm{Re}(\omega) < \omega_s$. Even when the resonance is unstable, we note that $\mathrm{Im}(\omega)$ is typically much smaller than the temporal growth rates of convective instabilities on an infinite plate (which for $\lambda = T = 0$ takes a maximum value of approximately 2×10^{-5}). In contrast, in figure 5 we plot $\mathrm{Im}(\omega)$ for family B, which are clearly temporally unstable, with a much stronger temporal growth rate than family A. The behaviour for much larger L will be discussed in the next subsection.

The asymptotic behaviour for larger $\mathrm{Re}(\omega)$ is confirmed in figure 3(*a*), in which each neutral resonance curve asymptotes to the curve (5.5) for each integer m (specimen asymptotes are plotted in figure 3*a*). Also plotted in figure 3(*a*) are the resonant lengths required for static divergence, equation (5.1). We note that if we follow a family-A resonance curve as ω increases, starting close to a static divergence with given n, then it joins onto a given real resonance curve which asymptotes to the same value $m = n$ in (5.5). Indeed each point of static divergence is connected to each neutral resonance curve via a family-A resonance. In contrast, the family-B resonances, while merging with each neutral resonance curve, appear to connect only to alternate static divergence points. We can hypothesise that the family-A and family-B resonances merge exactly at these static divergence points, but of course this cannot be verified explicitly within our scheme since we require $\mathrm{Re}(\omega)L/U \gg 1$.

It can be seen in figure 3(*b*) that the strongly unstable temporal resonances (family B) merge with the neutral resonances at a particular value of $\mathrm{Re}(\omega)$, which depends on the resonance curve under consideration and which decreases as L increases. These

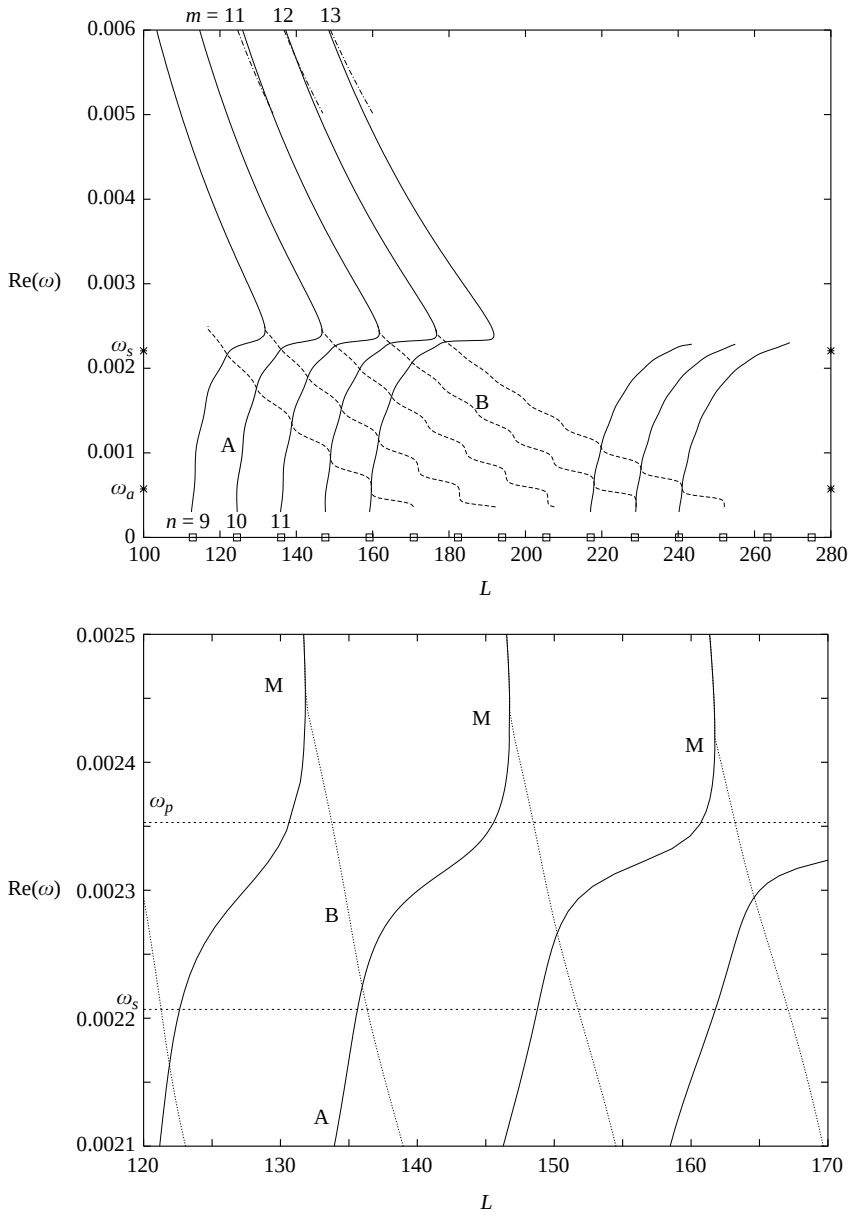

FIGURE 3. Variation of Re(ω) for resonant solutions against L. Here $U = 0.05$, $\lambda = U^5$ and $T = 0$. The solid lines denote Re(ω) for family A of complex modes and the dashed lines denote family B. The family-A resonances have complex frequency when $\omega_a < \mathrm{Re}(\omega) < \omega_s$ (marked by star symbols on the vertical axes), but otherwise have real frequency. Note that both families are repeated indefinitely for increasing L. In (a) the dash-dot lines correspond to the asymptotic resonance curves for larger Re(ω), equation (5.5), and the square symbols on the L-axis represent static-divergence, equation (5.1), with mode index n in the range 9 to 23, increasing from left to right. (b) A magnified view of a small portion of (a).

points are denoted by the letter M in figure 3(b), and correspond to the points to the right of figure 5 where $\mathrm{Im}(\omega) \to 0$. It is therefore concluded that the *finite* plate possesses flutter-type instabilities for a range of frequencies in excess of ω_s, for which

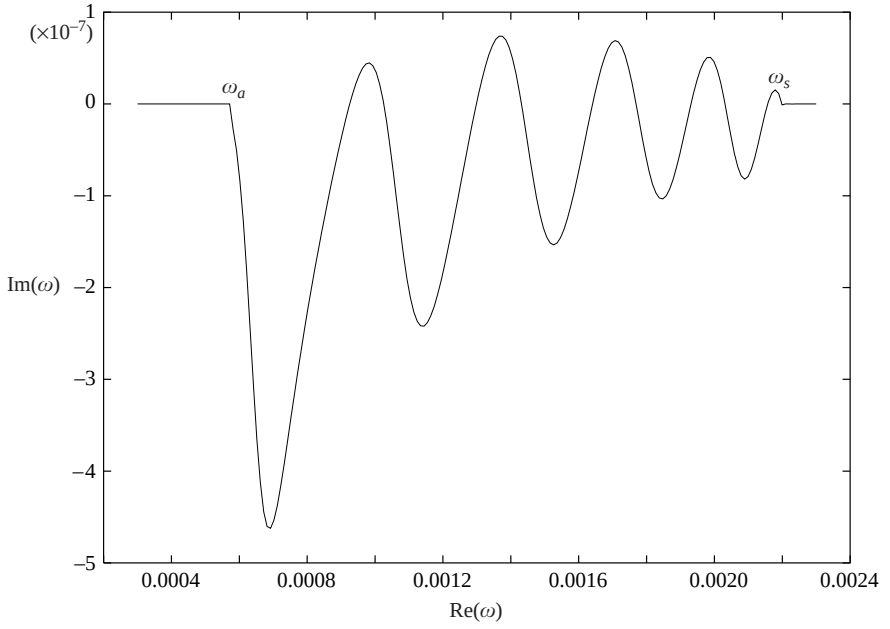

FIGURE 4. Plot of Im(ω) against Re(ω) for a representative family-A resonant solution (specifically the third from the right shown in figure 3*a*).

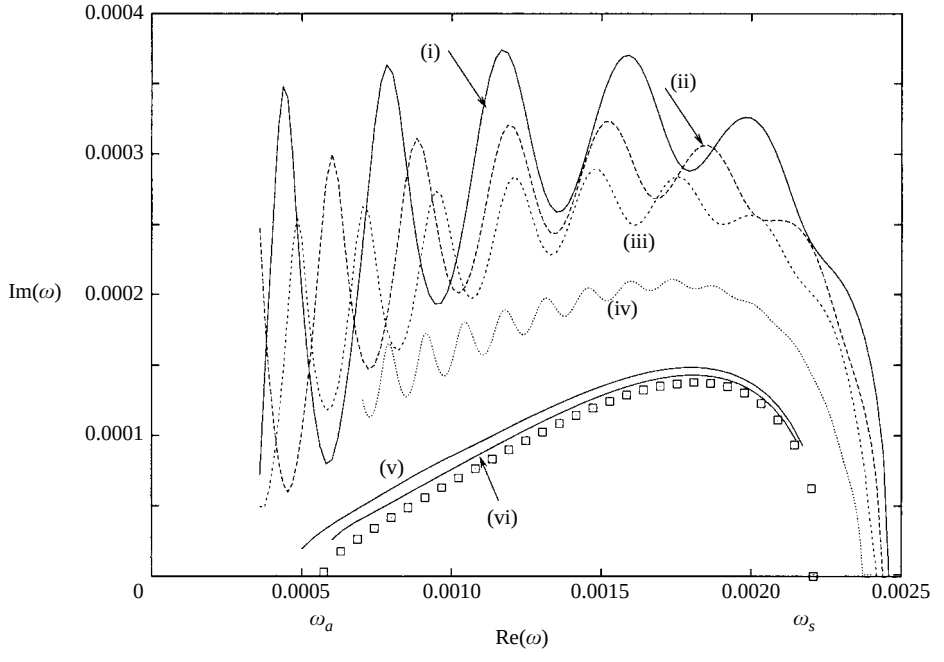

FIGURE 5. Plot of Im(ω) against Re(ω) for the resonant solutions from family B. The curves labelled (i)–(iii) correspond to the first, third and fifth family-B curves, working from left to right, in figure 3(*a*). Also shown are sample resonant solutions (iv)–(vi) for larger values of L – see text. The square symbols are the Kulikovskii condition (5.6). Note that for the sake of clarity the lower-frequency portion of curve (iv) has been omitted here.

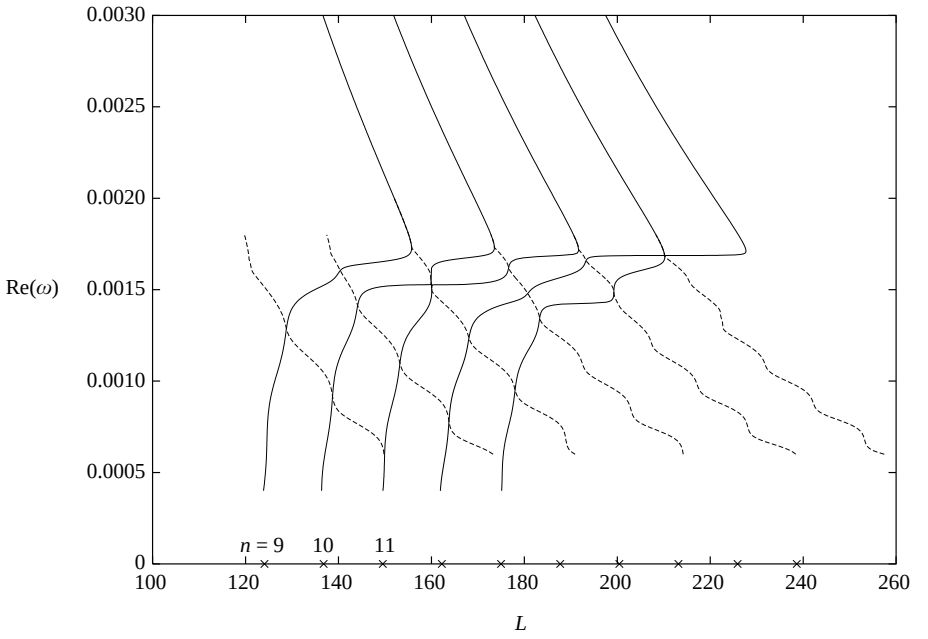

FIGURE 6. Conditions as in figure 3(*a*), but now with $T = 2U^2$. Solid lines are real resonances (family A), and dashed lines are complex resonances (family B). Note that both types of curve are repeated indefinitely for increasing L. The crosses on the horizontal axis correspond to static divergence, with index n in the range 9 to 18 shown – see equation (5.1).

the *infinite* plate is stable. The temporal growth rate of these instabilities is certainly greatest when a convectively unstable wave is present (i.e. for $\omega < \omega_s$, see figure 5), but is still non-zero for $\omega > \omega_s$ up to the points labelled M. (Note that the other crossing points in the Re(ω)–L plane shown in figure 3(*b*) do not correspond to the resonances coinciding, since the corresponding values of Im(ω) are not equal there.)

In figure 6 we have $T = 2U^2$, $\lambda = U^5$, for which the infinite plate is stable (figure 2*b*). The resonance curves are again repeated indefinitely for increasing L, and only a representative sample have been included. Two families of resonant curves are present. One family of curves have real frequencies, and correspond to family-A resonances seen for $T = 0$ in figure 3. A second family of resonance curves correspond to the family-B resonant curves seen for $T = 0$, and are again unstable – see figure 7. Note that at very low frequency in figure 6 both families of resonance curves approach points of static divergence, and that, just as for $T = 0$, the unstable B curves match only onto alternate static divergence points.

The significance of the results in figures 6 and 7 is that the finite plate is unstable even when the infinite plate is stable. Lucey & Carpenter (1992) have conducted a numerical experiment on the existence of divergence instability on an undamped finite plate, and have shown that divergence does indeed occur, in the form of a temporally growing disturbance with small, but non-zero, phase speed. In contrast, theories which study travelling waves on infinite plates, e.g. Landahl (1962), predict that divergence can only occur in the presence of damping. What we see here is confirmation of the Lucey & Carpenter result that damping is not required for instability, and this point will be discussed further in the final section.

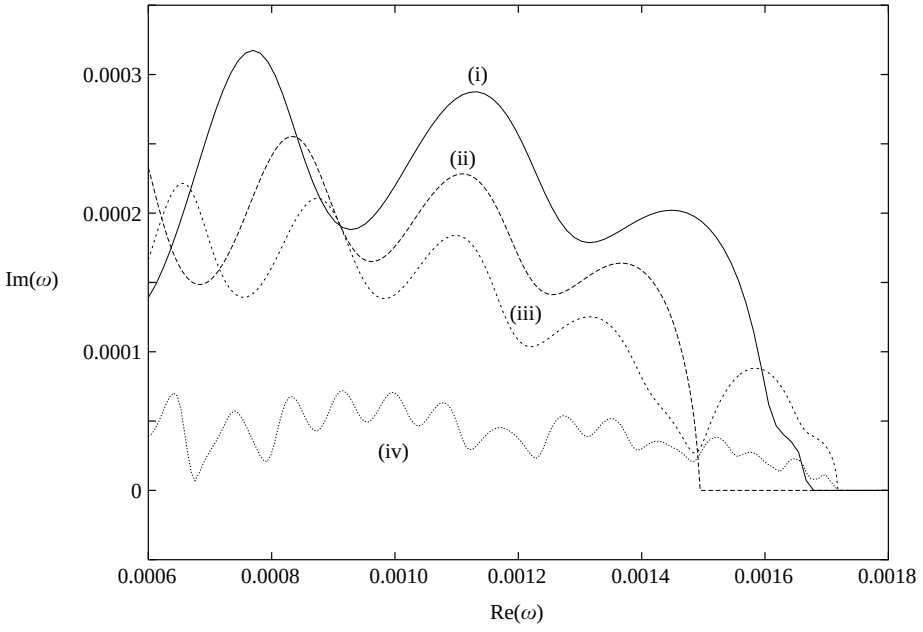

FIGURE 7. Plot of Im(ω) against Re(ω) for the complex resonant solutions from figure 6. The curves labelled (i)–(iii) correspond to the first, third and fifth dashed curves, working from left to right, in figure 6, respectively. Curve (iv) corresponds to a larger value of L – see text.

An interesting feature of both figures 3 and 6 is the rapid change in character of the *real* resonance curves as the resonance frequency passes through the range around ω_p. Of course, this is precisely the range over which the plate inertia, bending and mean flow terms in the dispersion relation are in balance, and provides the link between the static-type behaviour at very low frequency, and the behaviour at higher frequency in which the mean flow is less important. In certain cases two resonances appear exceedingly close together in parameter space. Note especially figure 6, for $L \approx 210$, where detailed inspection reveals that the two solid curves approach each other, but do not intersect. Presumably, some complicated dynamics could result if the system were forced at a frequency close to such a near-coincidence.

5.4. *The limit $L \to \infty$ when the infinite plate is unstable*

We will now consider what happens when L becomes very much larger than the values shown in figure 3. In this subsection we consider the case for which the infinite plate is convectively unstable.

It appears that the curves in figure 3, i.e. the behaviour of Re(ω) against L, simply repeat with largely unchanged form for longer and longer plates. However, the point labelled M in figure 3(b), corresponding to the point where the unstable resonance family B merges with the neutral resonances, certainly decreases, and appears to approach $\omega = \omega_s$ as L increases. In figure 5 we have also plotted Im(ω) for resonances at much higher values of L (specifically, the three curves labelled (iv),(v),(iv) in figure 5 correspond to resonance curves which pass through $L \approx 360, 2360, 4780$ respectively when Re(ω) = 0.002). For these larger values of L the Im(ω) curves approach the universal form indicated by the square symbols in figure 5.

In order to understand this behaviour, we note from equations (4.20) and (4.18) that the ij element of the matrix $\mathscr{S}^L \mathscr{S}^T$ contains exponential factors of the form

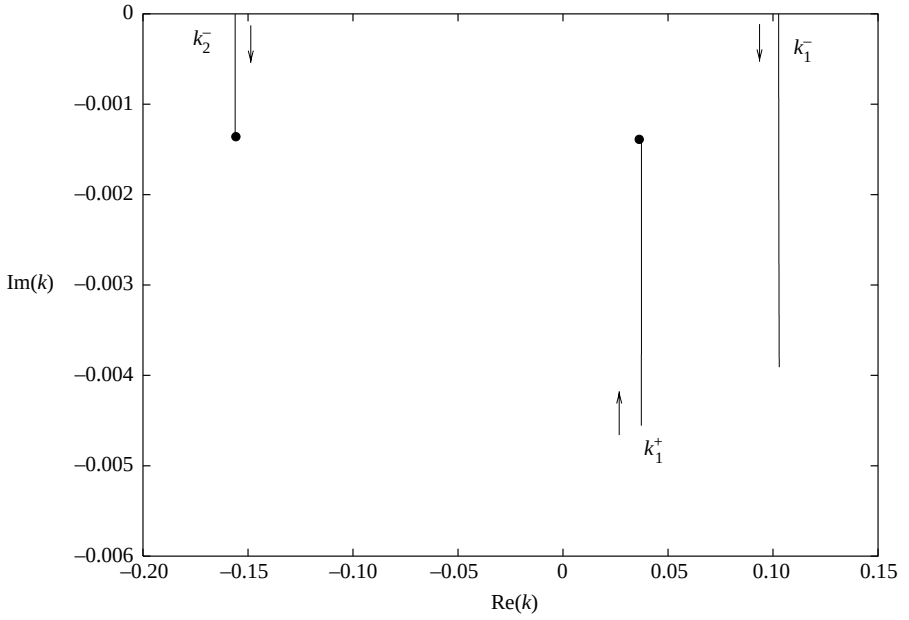

FIGURE 8. Plot of the motion of the infinite-plate wavenumbers in the complex-k-plane as $\mathrm{Im}(\omega)$ is increased from zero (in the direction of the arrows), for $T=0$, $U=0.05$, $\lambda=U^5$ and $\mathrm{Re}(\omega)=0.0018$. The filled circles indicate the point at which the Kulikovskii condition (5.6) is fulfilled.

$\exp(\mathrm{i}k_i^+L+\mathrm{i}k_j^+L-2\mathrm{i}k_k^-L)$ for $k=1,2$. Since the wavenumbers $k_{1,2}^{\pm}$ are in general all complex for ω complex, it follows that as $L\to\infty$ one of the factors $\exp(\mathrm{i}k_i^+L+\mathrm{i}k_j^+L-2\mathrm{i}k_k^-L)$ will become exponentially larger than the others. It is easy to see that this happens for $i=j=1$, since k_1^+ is the convectively unstable mode for $\mathrm{Re}(\omega)$ (and indeed $\mathrm{Im}(k_1^+)<\mathrm{Im}(k_2^+)$ for all $\mathrm{Im}(\omega)$). In order to satisfy the condition $\det(\mathscr{M})=0$, this largest exponential will have to balance with a term of unity arising from the identity matrix, and this in turn can only happen if the larger of $|\exp(2\mathrm{i}k_1^+L-2\mathrm{i}k_k^-L)|$ for $k=1,2$ is $O(1)$ for large L, i.e only if

$$\mathrm{minimum}_{k=1,2}\{\mathrm{Im}(k_1^+-k_k^-)\}=0. \tag{5.6}$$

Condition (5.6) is precisely the condition formulated by A. G. Kulikovskii (as cited in Landau & Lifshitz 1966, p. 281, and more recently described by Doare & de Langre (2002) in the context of the stability of a fluid-conveying pipe).

The idea is to vary $\mathrm{Im}(\omega)$ (in fact to increase it from zero), until condition (5.6) is satisfied. As $\mathrm{Im}(\omega)$ is increased, k_1^+ and $k_{1,2}^-$ move as shown in figure 8, and it turns out that (5.6) is satisfied with $k=2$, i.e. by the balance between the downstream convective instability and the upstream wave with negative phase velocity. The physical interpretation of (5.6) is clear: the resonance is being driven by the k_1^+ mode being scattered into the k_2^- mode at the trailing edge, and vice versa at the leading edge, with the temporal growth rate chosen so that the spatial growth achieved by the k_1^+ mode as it propagates downstream is exactly balanced by the spatial decay of the (in this case) k_2^- mode as it propagates back upstream. The growth rate predicted by (5.6) must always be less than the temporal growth rate for the convective instability on an infinite plate. The Kulikovskii condition itself is based purely on the stability properties of the infinite plate; the resonant selection of $\mathrm{Re}(\omega)$

still depends on the boundary conditions, but the selection of $\mathrm{Im}(\omega)$ is not influenced by the ends. This is because for a very long plate the energy exchange between the plate and the fluid along the plate length dominates over the energy exchange at the ends, so that as $L \to \infty$ the boundary conditions have a vanishing effect on the stability. The implication of this is that for plates with different end conditions, e.g. hinged–hinged or clamped–free ends, the stability properties as $L \to \infty$ are still given by (5.6), although of course for moderate L the end conditions can be expected to have a very significant effect.

The Kulikovskii condition (5.6) is plotted in figure 5, and is clearly in exceedingly close agreement with the numerical results for very large L. Note that for (5.6) we have that $\mathrm{Im}(\omega) \to 0$ as $\mathrm{Re}(\omega) \to \omega_{a,s}$. These points are of course the temporal stability thresholds for the infinite plate, at which the convective instability k_1^+ has become neutral, so that condition (5.6) is satisfied for $\mathrm{Im}(\omega) = 0$. As $L \to \infty$ instability will therefore occur in the range $\omega_a < \mathrm{Re}(\omega) < \omega_s$.

5.5. *The limit $L \to \infty$ when the infinite plate is stable*

As a final point we consider the case for which no convective instability is present on the infinite plate (figure 2*b*). Now the Kulikovskii condition (5.6) is satisfied for real frequency, since all four infinite-plate modes are then either neutral or evanescent. This implies that as $L \to \infty$ the resonances will approach zero growth rate, with the (now real) frequency still selected by the choice of L. In figure 7 (curve iv) we plot the growth rate along a resonance curve with large L – specifically, on this curve we have a resonance with $\omega = 0.0006 + \mathrm{i}0.000039$ when $L = 650.3$. Note that for large L the temporal growth rate is indeed reduced, and moreover it continues to be reduced as L is increased further. We will return to this point in the final section.

Of course, there is a fundamental difference between the cases of the infinite plate being unstable or stable. In the latter case the instability of our finite plate can be identified only with the presence of the boundaries, the effect of which diminishes as L increases. In the former case the instability also arises from the convective instability of one of the downstream waves, the effect of which will dominate the effect of the boundaries once L is very large indeed.

6. Wave energy

The concept of wave energy for waves on an infinite elastic plate was introduced by Landahl (1962) and Benjamin (1963), and is the amount of work done in building up a given wave, starting from rest at time $t = -\infty$. Cairns (1979) shows that it is equal to $\mathscr{E}|A|^2$, where $|A|$ is the wave amplitude and

$$\mathscr{E} = \frac{\omega}{4}\frac{\partial \mathscr{D}}{\partial \omega} = \frac{\omega}{2}\left[\omega + \frac{(\omega - kU)}{\gamma(k)}\right]. \tag{6.1}$$

Positive energy waves (PEWs, sometimes referred to as 'class B' disturbances) have $E > 0$, and behave conventionally in that they are stabilized by the introduction of dissipation, while negative energy waves (NEWs, or 'class A') have $E < 0$, and behave anomalously in that they are destabilized by the introduction of dissipation. In figure 2, the sign of the wave energy of each neutral mode can easily be checked: for instance, in figure 2(*a*) modes on the upper loop starting at $\omega = \omega_b$, and in figure 2(*b*) all of the upper branch, are PEWs; while in figure 2(*a*) modes on the lower branch from $\omega = \omega_b$ round to $\omega = 0$, and in figure 2(*b*) all of the lower branch with $\omega > 0$, are NEWs.

The above remarks all apply to waves on an infinite plate, and our aim in this section is to extend the concept of wave energy to our finite baffle. We consider throughout only eigenstates with real frequency, and such that each of the corresponding infinite-plate modes are real. Our first step is to add dashpot dissipation to the plate in order to destabilize the NEWs. This is achieved by including a term $\epsilon c_d \partial\eta/\partial t$ on the left-hand side of the plate equation (2.1). Here ϵc_d is the dashpot drag coefficient, c_d is positive and $O(1)$ and ϵ is taken to be small in order to ensure a slow build-up of the waves over a long timescale, defined to be $T_1 = \epsilon t$. We now consider the unsteady plate deflection expanded in the form

$$\eta(x, t) = [A(T_1)e(x) + \epsilon\eta_1(x, T_1)\ldots]\exp(-\mathrm{i}\omega t), \tag{6.2}$$

where $e(x)\exp(-\mathrm{i}\omega t)$ is an eigensolution of the homogeneous version of (2.8), for given real eigenfrequency ω. We then substitute this expansion into (2.8), and following the standard method of multiple scales replace $\partial/\partial t$ by $\partial/\partial t + \epsilon\partial/\partial T_1$. The resulting equation is automatically satisfied at $O(1)$, while at $O(\epsilon)$ we need to take a suitable inner product with $e(x)\exp(-\mathrm{i}\omega t)$. The inner product we choose is

$$\langle a, b\rangle = \int_{-L}^{L} a^* b \,\mathrm{d}x, \tag{6.3}$$

where the star superfix denotes complex conjugate. With respect to this inner product the operator $\mathscr{L}$ (together with the boundary conditions (2.6)) is self-adjoint, and without loss of generality we suppose that the eigenfunction is normalized such that $\langle e, e\rangle = 1$. We then find at $O(\epsilon)$ that

$$\frac{\mathrm{d}A}{\mathrm{d}T_1}\mathscr{E} + \frac{c_d\omega^2}{4}A = 0, \tag{6.4}$$

where $\mathscr{E} = \langle e, \mathscr{L}_\omega e\rangle\omega/4$, and $\mathscr{L}_\omega$ is the ω-derivative of the operator $\mathscr{L}$ at fixed frequency, i.e.

$$\mathscr{L}_\omega e(x) \equiv 2\omega e(x) - \frac{2}{\pi}\int_{-L}^{L} \ln|x-\xi|\left[\mathrm{i}U\frac{\partial e}{\partial \xi} + \omega e(\xi)\right]\mathrm{d}\xi. \tag{6.5}$$

It is shown in Appendix B that $\langle e, \mathscr{L}_\omega e\rangle$ is always real. Equation (6.4) can easily be solved to give $|A(T_1)| = |A(0)|\exp(-\omega^2 c_d T_1/4\mathscr{E})$, and hence the amplitude either decays or grows if $\mathscr{E}$ is positive or negative respectively. We can identify $\mathscr{E}$ as being the wave energy of our finite system, and equation (6.4) is readily interpreted as expressing the equality between the rate of change of the wave energy and the rate of working of the dashpots.

Equation (6.4) is exact for arbitrary values of L, and in order to simplify it we now use the fact that L is large, so that the eigenfunction $e(x)$ can be written as an expansion of infinite-plate waves over the outer region of the plate, in the form

$$e(x) \sim \sum_{i=1}^{4} \eta_i \exp(\mathrm{i}k_i x). \tag{6.6}$$

Here we have adopted for convenience a different notation than was used in the previous sections, in that we now number the modes 1–4 without reference to them being upstream or downstream. Note that for large L the contributions to the integral in (6.4) from the inner regions around each edge, where (6.6) is not valid, are neglected as asymptotically smaller than the contribution from the outer region. We substitute

(6.6) into (6.5), and using the expression for the generalized Fourier transform of the logarithm given in Lighthill (1958, p. 43),

$$\int_{-L}^{L} \ln|x-\xi| \exp(\mathrm{i}k\xi)\,\mathrm{d}\xi \sim -\frac{\pi}{\gamma(k)} \exp(\mathrm{i}kx) \quad \text{as} \quad L \to \infty, \tag{6.7}$$

find that

$$\mathscr{E} \approx \sum_{i,j=1}^{4} \eta_i \eta_j^* e_{ij} E_i. \tag{6.8}$$

Here e_{ij} is simply the inner product of two infinite-plate waves, given by

$$e_{ij} = \int_{-L}^{L} \exp(-\mathrm{i}k_j x + \mathrm{i}k_i x)\,\mathrm{d}x, \tag{6.9}$$

and E_i is the wave energy per unit length of a unit-amplitude wave $k = k_i$ on an infinite plate, i.e. from (6.1)

$$E_i = \frac{\omega}{2}\left[\omega + \frac{(\omega - k_i U)}{\gamma(k_i)}\right]. \tag{6.10}$$

The use of approximation (6.7) is only justified by our assumption that the plate is long on the scale of typical wavelengths. Now note that, since all the k_i are real,

$$e_{ij} = 2L\delta_{ij} + f_{ij}, \tag{6.11}$$

with δ_{ij} the Kronecker delta, and where f_{ij} can easily be shown to be $O(1)$ as $L \to \infty$. In our limit of large baffle length we can therefore make the approximation that the infinite-plate waves are orthogonal to leading order in L. This approximation relies on $|(k_i - k_j)|L \geqslant O(1)$ for $i \neq j$, and will therefore not hold close to the turning points $\omega = \omega_{s,p}$ (see figure 2), where two modes approach each other. Specifically, (6.11) will fail to hold if $|\omega - \omega_{s,p}| \leqslant O(L^{-2})$. If $e_{ij} \approx 2L\delta_{ij}$ does hold, however, it follows that

$$\mathscr{E} = 2L \sum_{i=1}^{4} |\eta_i|^2 E_i. \tag{6.12}$$

The wave energy, $\mathscr{E}$, is then simply the sum of the wave energies of the four constituent infinite-plate waves, weighted by the relative amplitude of those waves in the eigenstate under consideration. In the fictitious situation in which only one mode is present, say $\eta_1 = 1/\sqrt{2L}$, $\eta_i = 0$, $i \neq 1$, then $\mathscr{E}$ reduces exactly to Cairns' expression (6.1) for the wave energy. Of course, in reality all four wave modes will be present, due to the scattering at the leading and trailing edges.

Sample results are presented in figure 9 for some of the neutral resonant states shown in figure 3(*a*). For the cases considered here it is clear that $\mathscr{E}$ is negative for the frequency range $\omega_s < \omega < \omega_p$ over which NEWs exist on the infinite plate. It is by no means obvious that this would necessarily happen, since the wave energy of the finite plate is a superposition of contributions from both infinite-plate NEWS and PEWS, but it seems that in these cases the negative contributions dominate. These neutral resonances would therefore be destabilized by dissipation. The results shown in figure 9 have $T = 0$, but similar behaviour can be found for $T > 0$. In the next section we will show how tension induced by bending can affect the nonlinear evolution of the resonances.

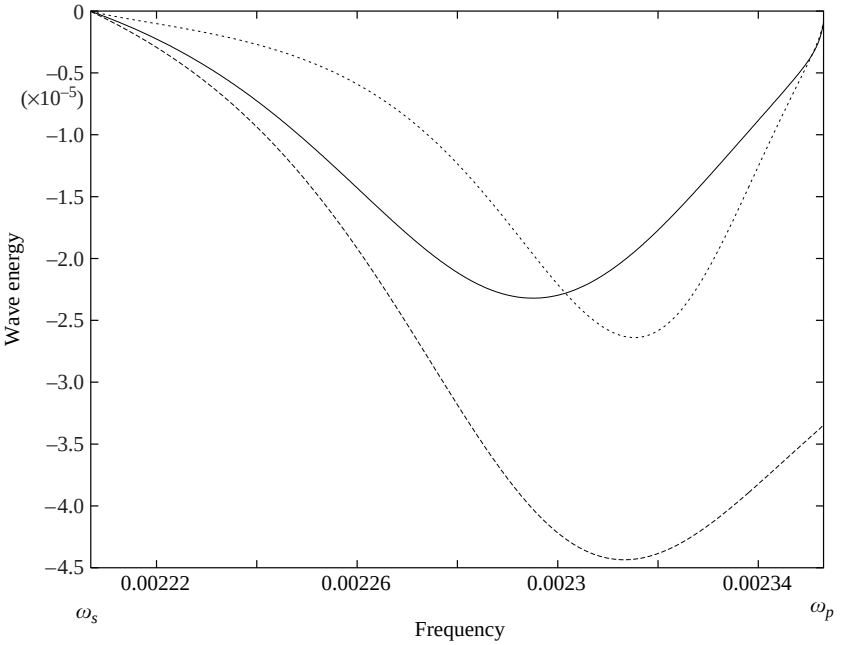

FIGURE 9. The variation of the wave energy, $\mathscr{E}$, from equation (6.12) against frequency, ω. The curves shown correspond to the neutral resonances shown in figure 3, specifically the three resonance curves $n = 9$ (solid), $n = 10$ (dashed) $n = 11$ (dotted) in figure 3a.

7. Nonlinear motion

In this section we will consider the nonlinear evolution of the states with negative wave energy described above. This has already been done for an infinitely long plate by Peake (2001), and our aim is to extend that work into the present finite-plate context. In Peake (2001) several nonlinear modifications to the plate and fluid equations are considered, but for a finite plate in a baffle the effect which will be most significant is the nonlinear tension induced by the bending of the plate. Using the non-dimensionalization described at the beginning of § 2, this nonlinear tension term takes the form

$$-\frac{\tau}{2L}\left(\int_{-L}^{L}\eta_{x'}^2\,\mathrm{d}x'\right)\frac{\partial^2\eta}{\partial x^2}, \tag{7.1}$$

where $\tau \equiv 6(1-\nu^2)(\rho_*^s/\rho_*^f)^2$, which is to replace the linear pre-tension term $-T\partial^2\eta/\partial x^2$ on the left-hand side of (2.1). Here ρ_*^s and ν are the plate density and Poisson ratio respectively. It is immediately clear that (7.1) is of exactly the same form as the linear pre-tension, but now with the tension determined by the total plate deflection. The key observation in what follows is that the nonlinear tension contains the factor $(\rho_*^s/\rho_*^f)^2$, which we take in this section only to be an asymptotically large parameter (for instance, approximately 50 for steel in water). In fact, we will choose the preferred scaling in which $\tau = \epsilon^{-2}\bar{\tau}$ with $\bar{\tau} = O(1)$.

Our idea here will be to destabilize a NEW eigenstate of the plate by adding small dashpot dissipation (amplitude $O(\epsilon) \ll 1$), as in the previous section, and then study the weakly nonlinear evolution of that state. As will be seen below, the eigenfrequency will depend on the nonlinear tension term, which in turn depends on the plate deflection, and it therefore follows that the eigenfrequency and the

eigenfunction must evolve over the slow timescale T_1 associated with the dashpot excitation. We therefore write

$$\eta(x,t) = \epsilon A(T_1) e(x,T_1) \exp\left(-\frac{\mathrm{i}}{\epsilon}\int^{T_1} \omega(T')\,\mathrm{d}T'\right) + \text{c.c.}, \tag{7.2}$$

with a similar expression for the fluid potential.

Equation (7.2) is now substituted into the equations (2.1–2.6), with the nonlinear term included in (2.1). At $O(1)$ we have that $\mathscr{L}[e(x,T) + \text{c.c.}] = 0$, with $\mathscr{L}$ having been modified by replacing the linear pre-tension by the nonlinear term, and where $\partial/\partial t$ has been replaced by $-\mathrm{i}\omega$. At $O(\epsilon)$ we then find that (including the resonant terms only)

$$\frac{\mathrm{d}}{\mathrm{d}T_1}[A\mathscr{L}_\omega e] - \frac{1}{2!}\frac{\mathrm{d}\omega}{\mathrm{d}T_1}[A\mathscr{L}_{\omega\omega} e] + c_d \omega A e = 0. \tag{7.3}$$

After a considerable amount of algebra, which is outlined in Appendix B, we arrive at

$$\frac{\mathrm{d}}{\mathrm{d}T_1}\left[|A|^2 \frac{\langle e, \mathscr{L}_\omega e\rangle}{4}\right] + \frac{c_d \omega}{2}|A|^2 = 0. \tag{7.4}$$

Here the term in square brackets can be identified as being precisely the wave action, while the second term arises from the dashpot dissipation. Of course, the conservation of wave action in the absence of dissipation is entirely to be expected – see Lighthill (1978). What is clear is that a static state, $(\mathrm{d}/\mathrm{d}T_1 \to 0)$, with non-zero amplitude can only exist if $\omega \to 0$ (static divergence). However, this does not mean that static divergence will necessarily be the long-time limiting solution of (7.4), as will be seen below.

Equation (7.4) has been derived without any approximation of large L. However, if we now introduce approximation (6.6), and further if we assume that we are in regimes in which the orthogonality condition $e_{ij} \sim 2L\delta_{ij}$ holds, then it is easy to show that at $O(1)$ the four allowed plate wavenumbers satisfy the nonlinear dispersion relation

$$\mathscr{D}(k_i, \omega, |A|) = w^2 + \frac{(\omega - k_i U)^2}{\gamma(k_i)} - k_i^4 - \mathscr{B}k_i^2 = 0. \tag{7.5}$$

Here

$$\mathscr{B} \equiv 2\bar{\tau}|A|^2 \sum_{j=1}^{4} |\eta_j|^2 k_j^2 \tag{7.6}$$

corresponds to the nonlinear tension. The resonant frequency is then determined, as a function of $\mathscr{B}$, exactly as in §4. At $O(\epsilon)$ we find that in (7.4) the wave action is $\mathscr{E}|A|^2/\omega$, with $\mathscr{E}$ given by approximation (6.12). This is the finite-plate version of the infinite-plate theory in Peake (2001). (Note that in Peake (2001) a number of other nonlinear terms were included in the plate equation and boundary conditions, but in the large-τ limit used here these terms will not affect equation (7.4).)

The frequency, $\omega = \omega(\mathscr{B})$, of our nonlinear oscillation is given by (7.5), and equation (7.4) then describes how the action evolves with T_1. It is therefore best to think of the action itself as being a function of $\mathscr{B}$, as is the modal amplitude $|A|$, so that (7.4) can be written as an evolution equation for $\mathscr{B}$ in the form

$$\frac{\mathrm{d}\mathscr{B}}{\mathrm{d}T_1} = -\frac{g(\mathscr{B})}{f'(\mathscr{B})}, \tag{7.7}$$

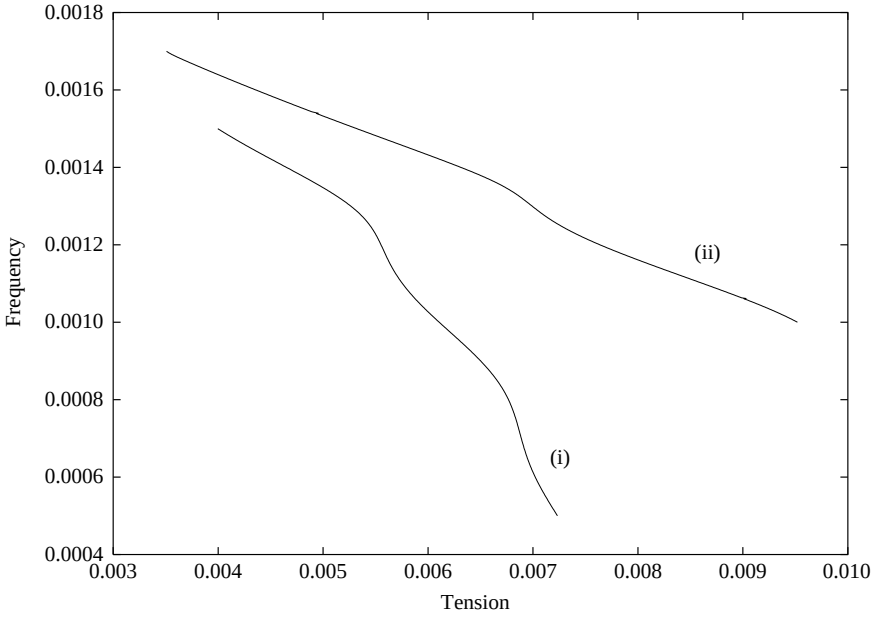

FIGURE 10. The variation of frequency ω against tension $\mathscr{B}$, for two different resonances. Here $U = 0.05$, $\lambda = U^5$, $L = 170$ and $\bar{\tau} = 1$. Labels (i) and (ii) match these curves to the corresponding curves in figure 11.

where $f(\mathscr{B}) = \mathscr{E}|A|^2/\omega$ is the action, the prime denotes differentiation with respect to $\mathscr{B}$ and $g(\mathscr{B})$ is the dashpot driving term, $g(\mathscr{B}) = c_d\omega|A|^2/2$. The variation of ω with $\mathscr{B}$ is shown in figure 10 for two representative resonance curves (note that the points where these curves pass through $\mathscr{B} = 2U^2 = 0.005$ match to the lower two points in figure 6 where $L = 170$, and also note that for the parameters chosen in figure 10 all four infinite-plate waves are neutral and the resonant frequencies are real). In figure 11 the corresponding variation of the action $f(\mathscr{B})$ is shown. Of course $g(\mathscr{B})$ is strictly positive, so that from figure 11 we can see that the solution of (7.7) is repelled from the maximum points of the action and is attracted to the minimum points as T_1 increases. The minimum point chosen, $\mathscr{B} = \mathscr{B}_1$ say, is the point which is accessible from the initial conditions, and will be reached in finite time, say at $T_1 = T_s$. It is easy to show that

$$|\mathscr{B} - \mathscr{B}_1| \propto |T_1 - T_s|^{1/2} \tag{7.8}$$

as $T_1 \to T_s$. Equation (7.4) breaks down as $T_1 \to T_s$, since the time derivative becomes unbounded. This singularity could be removed by choosing an inner timescale around $T_1 = T_s$ and introducing higher-order terms involving second-order derivatives. This will not be attempted here, because we note that these higher terms will not alter the fact that the solution of (7.4) is attracted to a minimum value of the wave action.

It is worth comparing the behaviour found here to that described by Peake (2001) for an infinite plate. For the infinite plate, one must consider a single wave of fixed wavelength, wavenumber k say, and then in order to introduce a nonlinear tension one must suppose that the plate is fixed to a series of hinges, a distance $2\pi/k$ apart, which allow only transverse motion. The nonlinear behaviour of the infinite plate is then described by the same plate equation as the finite baffle, but with length $2L$ replaced by $2\pi/k$. For the infinite plate, Peake (2001) found that for a NEW the

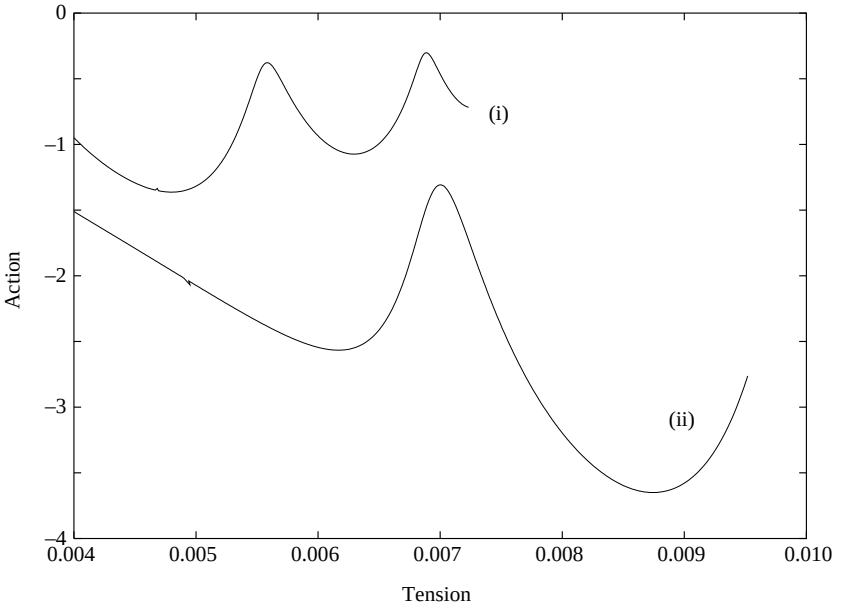

FIGURE 11. The variation of the wave action $f(\mathscr{B})$ corresponding to the curves (i) and (ii) in figure 10.

allowed oscillation frequency, ω, decreases monotonically as the nonlinear tension increases, exactly as it does for the finite baffle, as shown in figure 10. However, for the infinite plate the action (per unit amplitude) is simply $[\omega + (\omega - Uk)/k]/2$, and for a NEW is therefore a monotonically decreasing function of tension. This is in contrast to the action for the finite baffle, which we have shown can possess maxima and minima. For the infinite plate, dashpot dissipation will therefore act on a NEW so as to reduce ω (all the while making the action more negative), with $\omega \to 0$ as $T_1 \to \infty$. As $\omega \to 0$ the rate of working of the dashpot dissipation also approaches zero, and the system approaches a static saturated state in which the action is not extremized. For the finite baffle we have shown that quite different behaviour is possible, in that the dashpot dissipation will act to drive the system into a state of minimum action, in which the oscillation frequency and the rate of working of the driver are definitely non-zero. The difference in behaviour of the two systems must be due to the fact that the motion of the finite baffle over most of the plate length is made up of four waves, coupled by scattering at leading and trailing edges, as opposed to the single infinite-plate wave considered by Peake (2001). The total action then depends on the separate actions of each of these modes, and on the balance of their respective amplitudes, leading to the more complicated functional dependence of the action on tension shown in figure 11.

8. Summary and concluding remarks

In this paper we have been concerned with the resonant modes of a long finite elastic plate in the presence of uniform mean flow. A complicated picture has emerged, with several different families of modes being present. Consider first the linear theory:

(*a*) the undamped finite plate is temporally unstable, even in cases when the infinite plate is stable;

(*b*) in cases for which the infinite plate is convectively unstable, the temporal growth rate for a very long finite plate approaches a value which can be predicted from infinite-plate theory using the Kulikovskii condition;

(*c*) for neutral resonances a wave energy for the finite baffle has been derived, the sign of which predicts the plate response to structural damping. Despite the fact that the plate motion is a superposition of both NEWs and PEWS, it seems that for cases investigated this wave energy is negative.

Travelling-wave methods, such as Landahl (1962), predict that divergence instability on an infinite compliant wall must be excited by structural damping. However, for a finite wall Lucey & Carpenter (1992) have demonstrated numerically that no dissipation is required for divergence. Our analytical conclusion (*a*) above fully supports this. As Lucey & Carpenter (1993) argue, divergence on the finite plate arises from the de-phasing of the hydrodynamic pressure and wall normal velocity due to the presence of the edges. Specifically, if we consider motion with a single real frequency it is easy to see from (2.8) that in the absence of a line drive the rate of change of mechanical energy per unit plate length, averaged over an oscillation period, is equal to

$$-\frac{1}{2L}\int_{-L}^{L}\overline{p\frac{\partial\eta}{\partial t}}\,\mathrm{d}x, \tag{8.1}$$

where the overbar denotes time-average. For an infinite plate, pressure and wall deflection are exactly in phase, so that the time-average rate of working by the plate is zero, the mechanical energy is time-stationary and the oscillatory state is stable. However, this phasing is disrupted by the presence of the edges. Writing the plate deflection as $Ae(x)\exp(-\mathrm{i}\omega t)$ and using the large-L approximations set out in § 6, the quantity (8.1) becomes

$$\frac{\mathrm{i}\omega|A|^2}{8L}\sum_{i,j}\eta_i\eta_j^{*}f_{ij}\left\{\frac{(\omega-Uk_i)^2}{\gamma(k_i)}-\frac{(\omega-Uk_j)^2}{\gamma(k_j)}\right\}, \tag{8.2}$$

and we recall that f_{ij}, introduced in (6.11), is non-zero and $O(1)$ as $L\to\infty$. Note that the contribution from the isotropic term in (6.11) to the time average is zero. The appearance of f_{ij} corresponds to the fact that the baffle length is not in general equal to an exact, integer, number of full wavelengths for each of the four allowed infinite-plate waves. As argued by Lucey & Carpenter (1993), the presence of the edges means that there is a spatially dependent phase shift between the hydrodynamic pressure and the wall deflection. In our analysis this effect is very simply apparent from the fact that the plate deflection is a linear superposition of four plane waves, each wave with a different associated hydrodynamic pressure. The fact that the plate length is not an exact multiple of all four plate wavelengths then means that the rate of working integrated all along the whole plate is not exactly zero, leading to a non-zero total rate of change of mechanical energy, and hence to the possibility of instability. Note that our expansion of the plate deflection is invalid in the near field around each edge, which will make additional, finite contributions to the total rate of change of mechanical energy of the whole plate, and therefore $O(1/L)$ contributions to rate of change of mechanical energy per unit plate length. What is then clear from (8.2) is that the total rate of change of mechanical energy per unit length is $O(1/L)$ as $L\to\infty$, suggesting that divergence instability will progressively weaken as the plate is lengthened. Of course, for cases in which the infinite plate is convectively unstable, instability persists as $L\to\infty$ (point *b* above), but this occurs due to the growth of

the convectively unstable mode as it propagates along the plate, and not due to the de-phasing described by (8.2) above.

We wish to emphasize that although the infinite-plate solution has been used extensively in this paper, the solution we have obtained is for a genuinely *finite*, but long, plate. The infinite and finite plate cases are quite different, because the finite plate possesses ends which reflect the travelling waves with complex reflection coefficients of $O(1)$ amplitude, no matter how large L is. It therefore follows that taking the limit $L \to \infty$ in our solution does not reproduce the infinite-plate results, except in the case where a convective instability is present, which over the long plate then dominates the effects of the other waves. This explains why the total unsteady wall pressure and velocity, which are simply $\pi/2$ out of phase on an infinite plate, have a highly non-trivial phase relationship, and hence a non-zero rate of energy exchange between the fluid and the plate. The values of the reflection coefficients are determined here by solution of semi-infinite scattering problems, and emerge from the far-field limit of the complicated near-field interaction between a given incident wave and an edge.

Further parallels with Lucey & Carpenter's (1992) numerics can be drawn. We have already seen that our analytical results predict instability for zero wall damping. Further, Lucey & Carpenter observe a low-frequency instability – they choose a baffle length very close to the resonant lengths for static divergence, and it is clear from our figure 6 that in such a case our unstable mode would also have a *small* frequency (at least for baffle length just less than the static divergence lengths). Lucey & Carpenter also note that their divergence leads to growth all along the plate, and that is exactly what is seen here as well, thanks to the fact that our unstable modes possess a single temporal growth rate which is independent of x.

We turn now to the nonlinear analysis in § 7. Here we have derived an equation for the evolution of the finite-plate action in the presence of structural damping. In linear theory we saw in § 6 that states with negative wave energy are destabilized by damping, and the amplitude grows at constant frequency. However, once the nonlinear tension term is included the oscillation frequency must also be allowed to evolve in time. We see that the wave action is not a monotonic function of the plate nonlinear tension, but rather possesses distinct maxima and minima, at non-zero frequency, with the minima acting as attractors. The picture we then have is of an initial plate resonance of small amplitude and negative wave energy, which in the first instance grows in amplitude under the action of damping according to linear theory. The nonlinear behaviour then takes over and the solution reaches, in finite time, a saturated state of minimum action. This saturated state possesses a non-zero frequency, and a distinct wave amplitude. As we have already noted, this conclusion is quite different from the nonlinear behaviour of an infinite plate (Peake 2001), which is predicted to approach a state of *static* divergence under the action of damping. Similarly, Holmes (1978) proves that a fluid-conveying pipe cannot flutter, but will also approach static buckled equilibrium under the action of damping. Furthermore, Lucey *et al.* (1997) complete a numerical simulation of the nonlinear finite-baffle problem with spring backing. They indeed find here that static divergence is not observed in this case, and that nonlinear flutter-type waves are formed instead. This agrees with our prediction of a nonlinear fluttering motion of least action.

Finally, some comments may be made about the applicability of our long-plate assumption. The parameters used by Lucey *et al.* (1997) imply that the plate is long on a wavelength scale (see their figure 11). In fact, as pointed out by Carpenter & Garrad (1986, p. 223), the most unstable finite-plate modes have mode number proportional

to $L\lambda^{1/4}$, so that provided that $\lambda \neq 0$, the most unstable mode has a wavelength $O(1)$, i.e. $O(L)$ wavelengths fit along the plate, confirming the applicability of the long-plate assumption in this paper. A further point is that we require, among other conditions, $LU^{2/3} \gg 1$. For steel in water this condition reduces to $L_*/h_* \gg 58$ (specifically, with $\rho_*^f = 1000\,\mathrm{kg\,m^{-3}}$, Young's modulus $E_* = 21 \times 10^{10}\,\mathrm{N\,m^{-2}}$, Poisson ratio $\nu = 0.31$ and a flow speed of $10\,\mathrm{m\,s^{-1}}$). Alternatively, for the Kramer coating 'C' described by Carpenter & Garrad (1985, pp. 482, 483) we require only $L_*/h_* \gg 0.56$ (specifically, following Carpenter & Garrad, with $\rho_*^f = 1025\,\mathrm{kg\,m^{-3}}$, $E_* = 0.5 \times 10^6\,\mathrm{N\,m^{-2}}$, $\nu = 0.5$, $U_* = 18\,\mathrm{m\,s^{-1}}$). The much lower length/thickness ratio for the Kramer coating of course arises from the much lower value of E_*. The condition $LU^{2/3} \gg 1$ is therefore easily achieved in practice for the Kramer coating. In the case of steel in water, there is the question of how large $LU^{2/3}$ actually has to be to give reasonable results. Abrahams (1983, p. 228) has shown that the long-plate asymptotics predict the critical flow speed for divergence instability to within 2% of the 'exact' numerical value, even for the $n = 1$ mode in equation (5.1). This suggests that our asymptotic theory can give reasonable results in cases in which the thickness of the steel plate is no more than about 1% of the plate length, but of course this point will require much further investigation.

Appendix A

In this appendix we present the exact factorization of the Wiener–Hopf kernel $\mathscr{D}(k, \omega)$, in a form suitable for numerical evaluation. We start by writing $\mathscr{D}(k, \omega)$ in the form

$$\mathscr{D}(k,\omega) = -\left\{ \frac{-(\omega - Uk)^2 + \gamma(k)(k^4 - \omega^2 + Tk^2 + \lambda)}{\sqrt{k^2+N^2}\prod_{i=1}^{4}(k-k_i)} \right\} \frac{\sqrt{k^2+N^2}\prod_{i=1}^{4}(k-k_i)}{\gamma(k)}. \quad \text{(A 1)}$$

The function in curly brackets is denoted as $E(k)$, which is factorized in the form $E(k) = E^+(k)E^-(k)$, with $E^\pm(k)$ analytic and non-zero in the upper and lower half-planes $R^\pm$ respectively. This is completed using the Cauchy-integral formula

$$E^\pm(k) = \exp\left[\frac{\pm 1}{2\pi \mathrm{i}} \int \frac{\ln(E(\xi))}{\xi - k} \mathrm{d}\xi \right]; \quad \text{(A 2)}$$

see Noble (1988, p. 15). In principle, the integration contour lies along the intersection of $R^\pm$, but in practice is deformed back onto the real axis, necessitating possible inclusion of a residue contribution from the pole at $\xi = k$. For instance, if we require $E^+(k_{1,2}^+)$ for real frequencies for which $k_{1,2}^+$ are real, then the integration contour is the real axis, indented below the real simple pole at $\xi = k_{1,2}^+$, and the integral is then computed as a (half) residue contribution from the simple pole plus a Cauchy principle value integral along the real axis. Note that the form of $E(k)$ in (A 1) has been chosen to ensure that $E(k)$ is non-zero (particularly on the integration contour), that $E(k) \to 1$ as $k \to \infty$ (so the integral is well-behaved at infinity), and so that $E(k)$ is well-behaved near $k = 0$.

The integrals in our expressions for $E^\pm(k)$ can be computed using standard numerical routines. Once the factors of $E(k)$ have been calculated, the remaining terms in (A 1) can be factorized exactly. Note that the term $\sqrt{k^2+N^2}$ has been included in (A 1) so as to give $E(k)$ the correct behaviour at infinity, with N a fixed

constant. The branch cuts associated with $\sqrt{k^2+N^2}$ emanate from $\pm \mathrm{i}N$ and run parallel to the imaginary axis through upper and lower half-planes respectively. The value of N is chosen so that the branch points lie well away from the integration contour, which is achieved in most cases by setting $N=1$. It follows that

$$\mathscr{D}^{\pm}(k,\omega) = \mathrm{i}E^{\pm}(k)\frac{\displaystyle\prod_{j=1}^{2}(k-k_j^{\mp})\sqrt{k\pm\mathrm{i}N}}{\sqrt{k\pm\mathrm{i}\epsilon}}; \tag{A 3}$$

note again that the appropriate branch cuts join the branch points in $\mathscr{D}^{\pm}(k,\omega)$ to infinity from the lower/upper half-planes respectively, a point emphasized by writing $\gamma(k)$ as $\sqrt{k^2+\epsilon^2}$ with $\epsilon \to 0$.

Appendix B

In this appendix we outline the steps required between equation (7.3) and (7.4). We take the inner product of (7.3) with Ae, and add the resulting equation onto its own complex conjugate. This leads to

$$\frac{\mathrm{d}}{\mathrm{d}T_1}\left\{|A|^2[\langle e, \mathscr{L}_\omega e\rangle + \text{c.c.}]\right\} - \left\{\langle e, \mathscr{L}_\omega e\rangle A\frac{\mathrm{d}A^*}{\mathrm{d}T_1} + \text{c.c.}\right\}$$
$$-|A|^2\left\{\left\langle \frac{\mathrm{d}e}{\mathrm{d}T_1}, \mathscr{L}_\omega e\right\rangle + \text{c.c.}\right\} + \frac{|A|^2}{2}\frac{\mathrm{d}\omega}{\mathrm{d}T_1}\{\langle e, \mathscr{L}_{\omega\omega}e\rangle + \text{c.c.}\} + 2\omega c_d|A|^2 = 0. \tag{B 1}$$

We now manipulate this equation as described below.

First, we note from (6.5) that

$$\langle e, \mathscr{L}_\omega e\rangle - \langle e, \mathscr{L}_\omega e\rangle^* = -\frac{2\mathrm{i}U}{\pi}\int_{-L}^{L}\int_{-L}^{L}\ln|x-\xi|\left\{e^*(x)\frac{\partial e(\xi)}{\partial \xi} - e(x)\frac{\partial e^*(\xi)}{\partial \xi}\right\}\mathrm{d}\xi\,\mathrm{d}x. \tag{B 2}$$

In the second term in (B 2) we use integration by parts in the ξ-integral (together with the boundary condition (2.6)) to shift the ξ-derivative onto the logarithm, use the symmetry of the argument of the logarithm to convert this into an x-derivative, use integration by parts once more to shift the x-derivative onto the $e(x)$, and finally swap ξ and x. After this manipulation the second term on the right-hand side of (B 2) cancels exactly with the first, demonstrating that $\langle e, \mathscr{L}_\omega e\rangle$, and hence the wave action, is real. A similar argument can be used to show that $\langle e, \mathscr{L}_{\omega\omega} e\rangle$ is also real.

Second, using exactly the same sorts of manipulation as described at the end of the last paragraph, it can be shown that

$$|A|^2\left\{\left\langle \frac{\mathrm{d}e}{\mathrm{d}T_1}, \mathscr{L}_\omega e\right\rangle + \left\langle \mathscr{L}_\omega e, \frac{\mathrm{d}e}{\mathrm{d}T_1}\right\rangle\right\} = -\frac{2\omega|A|^2}{\pi}\frac{\mathrm{d}}{\mathrm{d}T_1}\left\langle e, \int_{-L}^{L}\ln|x-\xi|e(\xi)\mathrm{d}\xi\right\rangle$$
$$-\frac{2\mathrm{i}U|A|^2}{\pi}\frac{\mathrm{d}}{\mathrm{d}T_1}\left\langle e, \int_{-L}^{L}\ln|x-\xi|\frac{\partial e(\xi)}{\partial \xi}\mathrm{d}\xi\right\rangle, \tag{B 3}$$

and after some straightforward manipulation, and use of the fact that $\langle e, e\rangle = 1$, we find that the quantity on the right of (B 3) is

$$|A|^2\frac{\mathrm{d}}{\mathrm{d}T_1}[\langle e, \mathscr{L}_\omega e\rangle] - |A|^2\frac{\mathrm{d}\omega}{\mathrm{d}T_1}[\langle e, \mathscr{L}_{\omega\omega}e\rangle]. \tag{B 4}$$

We can now use equation (B 4) to yield (7.4) from (B 1).

REFERENCES

Abrahams, I. D. 1981 Scattering of sound by a heavily loaded finite elastic plate. *Proc. R. Soc. Lond.* A **378**, 89–117.

Abrahams, I. D. 1983 Scattering of sound by an elastic plate with flow. *J. Sound Vib.* **89**, 213–231.

Abrahams, I. D. & Wickham, G. R. 2001 On transient oscillations of plates in moving fluids. *Wave Motion* **33**, 7–23.

Benjamin, T. B. 1963 The threefold classification of unstable disturbances in flexible surfaces bounding inviscid flows. *J. Fluid Mech.* **16**, 436–450.

Bers, A. 1983 Space-time evolution of plasma instabilities – absolute and convective. In *Handbook of Plasma Physics* (ed. M. N. Rosenbluth & R. Z. Sagdeev), vol. 1, pp. 451–517. North-Holland.

Brazier-Smith, P. R. & Scott, J. F. 1984 Stability of fluid flow in the presence of a compliant surface. *Wave Motion* **6**, 547–560.

Briggs, R. J. 1964 *Electron-stream Interaction with Plasmas*. MIT Press.

Cairns, R. A. 1979 The role of negative energy waves in some instabilities of parallel flows. *J. Fluid Mech.* **92**, 1–14.

Cannell, P. A. 1976 Acoustic edge scattering by a heavily loaded elastic half-plane. *Proc. R. Soc. Lond.* A **350**, 71–89.

Carpenter, P. W. & Garrad, A. D. 1985 The hydrodynamic stability of flow over Kramer-type compliant surfaces. Part 1. Tollmien–Schlichting instabilities. *J. Fluid Mech.* **155**, 465–510.

Carpenter, P. W. & Garrad, A. D. 1986 The hydrodynamic stability of flow over Kramer-type compliant surfaces. Part 2. Flow-induced surface instabilities. *J. Fluid Mech.* **170**, 199–232.

Crighton, D. G. & Innes, D. 1984 The modes, resonances and forced response of elastic structures under heavy fluid loading. *Phil. Trans. R. Soc. Lond.* A **312**, 295–341.

Crighton, D. G. & Oswell, J. E. 1991 Fluid loading with mean flow. I. Response of an elastic plate to localized excitation. *Phil. Trans. R. Soc. Lond.* A **335**, 557–592.

Doare, O. & de Langre, E. 2002 Local and global instability of fluid-conveying pipes on elastic foundations. *J. Fluids Struct.* **16**, 1–14.

Dowell, E. H. 1975 *Aeroelasticity of Plates and Shells*. Noordhoff.

Ellen, C. H. 1973 The stability of simply supported rectangular surfaces in uniform subsonic flow. *Trans. ASME: J. Appl. Mech.* **40**, 68–72.

Ellen, C. H. 1977 The non-linear stability of panels in incompressible flow. *J. Sound Vib.* **54**, 117–121.

Holmes, P. J. 1978 Pipes supported at both ends cannot flutter. *Trans. ASME: J. Appl. Mech.* **45**, 619–622.

Junger, M. C. & Feit, D. 1986 *Sound, Structures, and Their Interaction*. MIT Press.

Kelbert, M. & Sazonov, I. 1996 *Pulses and Other Processes in Fluids*. Kluwer.

Kornecki, A. 1974 Static and dynamic instability of panels and cylindrical shells in subsonic potential flow. *J. Sound Vib.* **32**, 251–263.

Kramer, M. O. 1960 Boundary layer stabilisation by distributed damping. *J. Am. Soc. Nav. Engrs.* **72**, 25–33.

Landahl, M. T. 1962 On the stability of a laminar incompressible boundary layer over a flexible surface. *J. Fluid Mech.* **13**, 609–632.

Landau, L. & Lifshitz, E. 1966 *Course of Theoretical Physics, Physical Kinetics*, Vol. 10. Oxford.

de Langre, E. 2002 Absolutely unstable waves in inviscid hydorelastic systems *J. Sound Vib.* **256**, 299–317.

Lighthill, M. J. 1958 *An Introduction to Fourier Analysis and Generalised Functions*. Cambridge University Press.

Lighthill, M. J. 1978 *Waves in Fluids*. Cambridge University Press.

Lucey, A. D. 1998 The excitation of waves on a flexible panel in a uniform flow. *Phil. Trans. R. Soc. Lond.* **356**, 2999–3039.

Lucey, A. D., Cafolla, G. J., Carpenter, P. W. & Yang, M. 1997 The nonlinear hydroelastic behaviour of flexible walls. *J. Fluids Struct.* **11**, 717–744.

Lucey, A. D. & Carpenter, P. W. 1992 A numerical simulation of the interaction of a compliant wall with inviscid flow. *J. Fluid Mech.* **234**, 121–146.

Lucey, A. D. & Carpenter, P. W. 1993 On the difference between the hydroelastic instability of infinite and very long compliant panels. *J. Sound Vib.* **163**, 176–181.

Noble, B. 1988 *Methods Based on the Wiener–Hopf Technique*. 2nd Ed. Chelsea.

Oswell, J. E. 1992 Fluid loading with mean flow. PhD Thesis, Cambridge University, UK.

Peake, N. 2001 Nonlinear stability of a fluid-loaded elastic plate with mean flow. *J. Fluid Mech.* **434**, 101–118.